Reviews of Geophysics

AMERICAN GEOPHYSICAL UNION

VOLUME 45 NUMBER 2 JUNE 2007

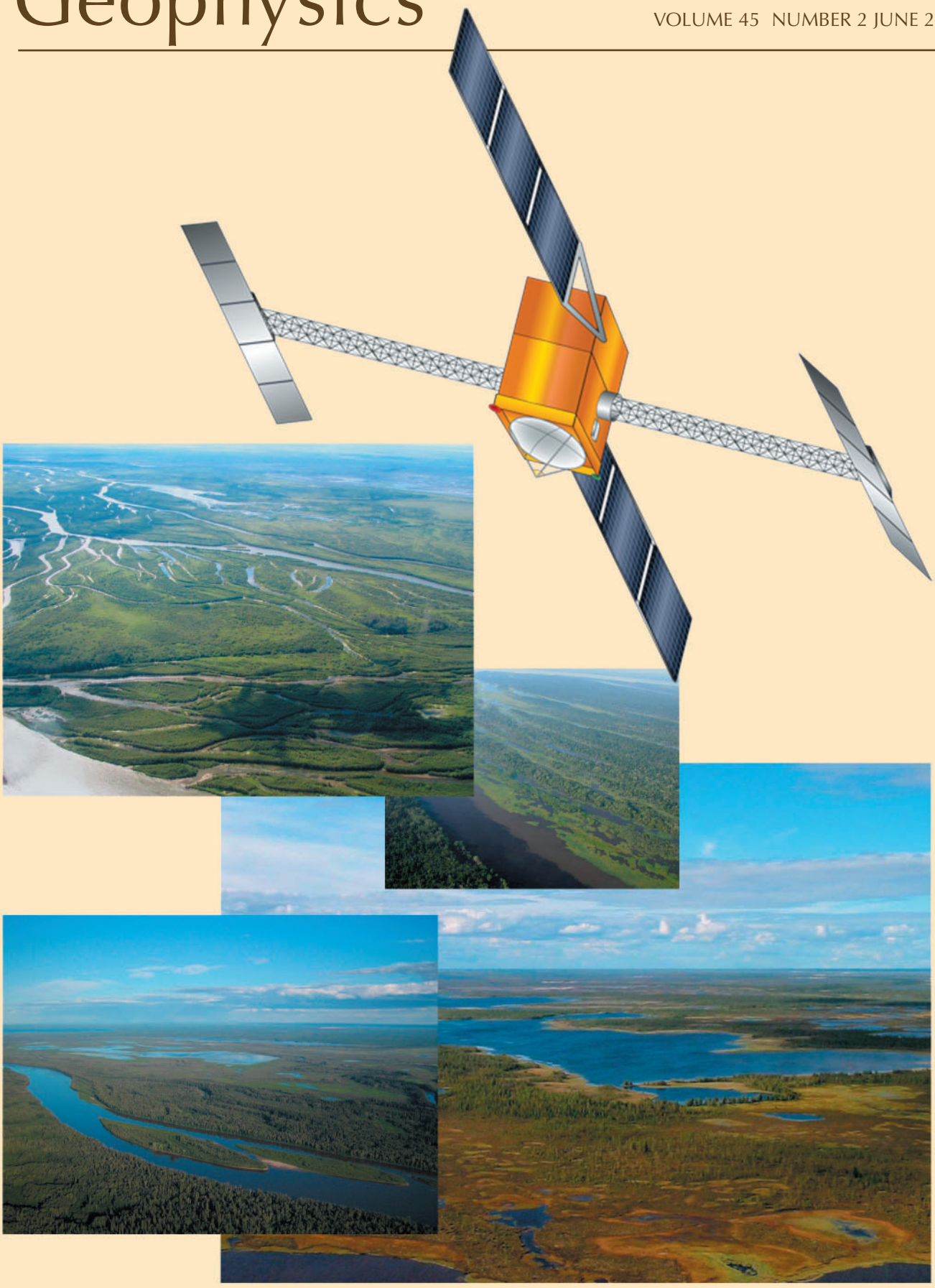

# MEASURING SURFACE WATER FROM SPACE

Douglas E. Alsdorf,[1] Ernesto Rodríguez,[2] and Dennis P. Lettenmaier[3]

Received 1 February 2006; revised 7 August 2006; accepted 17 November 2006; published 9 May 2007.

[1] Surface fresh water is essential for life, yet we have surprisingly poor knowledge of the spatial and temporal dynamics of surface freshwater discharge and changes in storage globally. For example, we are unable to answer such basic questions as "What is the spatial and temporal variability of water stored on and near the surface of all continents?" Furthermore, key societal issues, such as the susceptibility of life to flood hazards, cannot be answered with the current global, in situ networks designed to observe river discharge at points but not flood events. The measurements required to answer these hydrologic questions are surface water area, the elevation of the water surface ($h$), its slope ($\partial h/\partial x$), and temporal change ($\partial h/\partial t$). Advances in remote sensing hydrology, particularly over the past 10 years and even more recently, have demonstrated that these hydraulic variables can be measured reliably from orbiting platforms. Measurements of inundated area have been used to varying degrees of accuracy as proxies for discharge but are successful only when in situ data are available for calibration; they fail to indicate the dynamic topography of water surfaces. Radar altimeters have a rich, multidecadal history of successfully measuring elevations of the ocean surface and are now also accepted as capable tools for measuring $h$ along orbital profiles crossing freshwater bodies. However, altimeters are profiling tools, which, because of their orbital spacings, miss too many freshwater bodies to be useful hydrologically. High spatial resolution images of $\partial h/\partial t$ have been observed with interferometric synthetic aperture radar, but the method requires emergent vegetation to scatter radar pulses back to the receiving antenna. Essentially, existing spaceborne methods have been used to measure components of surface water hydraulics, but none of the technologies can singularly supply the water volume and hydraulic measurements that are needed to accurately model the water cycle and to guide water management practices. Instead, a combined imaging and elevation-measuring approach is ideal as demonstrated by the Shuttle Radar Topography Mission (SRTM), which collected images of $h$ at a high spatial resolution ($\sim$90 m) thus permitting the calculation of $\partial h/\partial x$. We suggest that a future satellite concept, the Water and Terrestrial Elevation Recovery mission, will improve upon the SRTM design to permit multitemporal mappings of $h$ across the world's wetlands, floodplains, lakes, reservoirs, and rivers.

**Citation:** Alsdorf, D. E., E. Rodríguez, and D. P. Lettenmaier (2007), Measuring surface water from space, *Rev. Geophys.*, *45*, RG2002, doi:10.1029/2006RG000197.

## 1. INTRODUCTION

[2] Given societies' basic need for fresh water, perhaps the most important hydrologic observations that can be made are of the temporal and spatial variations in water stored in rivers, lakes, reservoirs, floodplains, and wetlands. There is a widespread recognition of the need for better observations and understanding of surface water distribution globally [e.g., *Marburger and Bolten*, 2004, 2005; *United Nations*, 2004; *International Working Group on Earth Observations*, 2005; *National Science and Technology Council*, 2004] especially in view of the fact that over one third of the world's population is not served by adequate supplies of clean water [*Gleick*, 2003]. Existing in situ networks, notwithstanding that they have served well water development needs in the industrialized world, do not provide an adequate global knowledge base of the changes in the volume of water stored and flowing in rivers, lakes, and wetlands (see sections 2 and 3). Furthermore, the spatial extent and variability of wetlands, lakes, reservoirs, and other water bodies are poorly known globally, even though they strongly affect biogeochemical and trace gas fluxes between the land and atmosphere and transport to the oceans [e.g., *Richey et al.*, 2002; *Frey and Smith*, 2007]. Lacking global observations of surface water dynamics leads to several basic questions (section 3). Perhaps the most fundamental is, "What is the spatial and temporal variability in terrestrial surface water storage, and how can we predict these variations more accurately?" We expand on the scientific and societally relevant questions in section 3 and detail the hydrologic measurement and

[1]School of Earth Sciences, Ohio State University, Columbus, Ohio, USA.
[2]Jet Propulsion Laboratory, California Institute of Technology, Pasadena, California, USA.
[3]Department of Civil and Environmental Engineering, University of Washington, Seattle, Washington, USA.



8755-1209/07/2006RG000197$15.00
Paper number 2006RG000197

modeling requirements necessary for answering the questions in sections 4 and 5, respectively.

[3] Recognizing the potential scientific and applications benefits of satellite-based surface water observations, NASA's Terrestrial Hydrology Program formed a Surface Water Working Group (SWWG) in 1999 to foster the development of spaceborne technologies capable of collecting global surface water measurements that would help fill these voids in global surface water observations [*Alsdorf et al.*, 2003; *Alsdorf and Lettenmaier*, 2003]. A community of researchers throughout Europe met at the "Hydrology from Space" workshop at the French space agency (Centre National d'Etudes Spatiales) in Toulouse on September 2003 and initiated similar actions [*Cazenave et al.*, 2004]. This international community supports global efforts to provide both the measurement technology and hydrologic science infrastructures necessary for spaceborne missions. In section 6 we describe a potential future mission scenario that has developed from these meetings.

## 2. DIFFICULTIES WITH IN SITU MEASUREMENTS

[4] In situ gauge measurements are the backbone of the current understanding of global surface water dynamics. They have helped to quantify the movement of water (discharge) in river channels but provide comparatively little information about the spatial dynamics of surface water extent, such as floodplain flows and the dynamics of wetlands. In situ methods essentially provide a one-spatial-dimension, point-based view of water surfaces that is appropriate in situations where a well-defined channel boundary confines the flow but not in more complex riverine environments that involve movement of water over wetlands and floodplains, which include both diffusive flows and multiple, narrow, confined (channel) hydraulics. This complexity is fundamentally a three-spatial-dimension process varying in space and time, which cannot be sampled adequately with one-spatial-dimension observation protocols.

[5] Observations of river stage (height) have been collected over much of the developed world's river basins for over half a century; however, stream gauge network densities in the nonindustrialized nations are generally much sparser. For example, surface water across much of Africa and portions of the Arctic is either not measured or is measured extremely sparsely, especially given the loss of many stream gauges in the former Soviet Union and elsewhere over the last 2 decades [*Vörösmarty et al.*, 2001; *Stokstad*, 1999; *Shiklomanov et al.*, 2002]. Even in places where stream gauges exist, legal and institutional restrictions often make the data unavailable for scientific purposes. Two examples illustrate the magnitude of the problem. (1) The area surrounding Washington D. C., includes about 700 stream gauges, some on the Potomac River, which has an annual average discharge of $\sim$400 $m^3/s$. Yet the same amount of area centered on Manaus in the central Amazon Basin includes about 10 gauges, and the Negro River with its $\sim$40,000 $m^3/s$ annual average flow is almost completely ungauged. Essentially, the gauge density (expressed as number of gauges per unit discharge) in the Amazon is roughly 4 orders of magnitude less than a typical area in the eastern United States. Furthermore, the few Amazon gauges that do exist are useful only for estimation of flow in the major river channels; they provide no information about the dynamics of storage and discharge variations in the extensive near-river wetland system. (2) The mean interannual storage variation in five of Africa's largest lakes is $\sim$200 mm (where area is normalized such that volumes are represented as height variations), as measured from TOPEX/Poseidon radar altimetry overlaid on an advanced very high resolution radiometer (AVHRR) land classification [*Sridhar et al.*, 2003; *Mercier et al.*, 2002]. When normalized to the land area of Africa, this variation is about one tenth of the model-based estimate of the mean seasonal cycle in soil moisture averaged over the continent. It is expected that when storage changes in all of Africa's lakes, reservoirs, and wetlands are included, the variability in surface water storage may well approach that of soil moisture.

[6] We argue that our "ability to measure, monitor, and forecast U.S. and global supplies of fresh water" [*Marburger and Bolten*, 2004, 2005] using in situ methods is essentially impossible because of (1) the physics of water flow across floodplains, wetlands, and other areas that are not well constrained by defined channel networks, (2) the decline in the numbers of gauges worldwide, and (3) the poor economies and infrastructure problems that exist for nonindustrialized nations. Given that rivers and wetlands cover well over 4% of the Earth's surface [*Prigent et al.*, 2001; *Matthews and Fung*, 1987] and up to 20% of humid basins such as the Amazon [*Hess et al.*, 2003; *Richey et al.*, 2002], the implications of the problem are global.

## 3. SCIENCE AND APPLICATIONS QUESTIONS

[7] Spaceborne measurements of terrestrial surface waters provide unique capabilities to address the following questions in ways that are not possible with existing (or any reasonably feasible expansion of) in situ gauge networks.

### 3.1. Global Water and Energy Cycles

[8] Global models of weather and climate could be constrained spatially and temporally by stream discharge and surface storage measurements. Yet this constraint is rarely applied, despite modeling results showing that precipitation predicted by weather forecast models is often inconsistent with observed discharge. For example, *Roads et al.* [2003] performed a comprehensive assessment of global and regional weather forecast models, using their predicted precipitation over the Mississippi River basin and routing the runoff produced by their land surface schemes to the mouth of the Mississippi River. They found that the resulting model predictions of streamflow were often in error by 50%, and even 100% mismatches with observations were not uncommon. *Coe* [2000] found similar results for climate model predictions of the rainfall-related discharge over many of the world's large rivers. Given that river discharge

**Figure 1.** Inundated floodplain of the Amazon River. This geomorphology is highly complex, lacking well-defined channels; rather diffusive flow conditions are prevalent. Stream gauges are incapable of measuring these flow conditions and related storage changes. In fact, in situ gauges are not present anywhere on the Amazon floodplain. Photograph courtesy of L. Hess.

represents ~40% of precipitation over global land areas, such large errors in runoff prediction imply large errors in the models' representation of evapotranspiration, and hence surface energy fluxes, as well. Better observations in real time of the dynamics of the global rivers therefore have considerable potential for improving both weather and climate prediction.

[9] Interseasonal and interannual variations in surface water storage volumes as well as their impact on precipitation, evaporation, infiltration, and runoff are not well known. The terrestrial water balance equation used in hydrologic models and as applied to a river basin is

$$\mathbf{P} - \mathbf{E} = Q_s + Q_g + d\mathbf{S}/dt, \quad (1)$$

where **P** and **E** are basin-averaged precipitation and evaporation, respectively; $Q_s$ is river discharge; $Q_g$ is groundwater discharge across the basin boundary; $t$ is time, and **S** is the total surface and subsurface storage (summed from soil moisture, snow water content, surface water storage, vegetation water content, groundwater, and glaciers [e.g., *Lettenmaier*, 2005]). Each of the variables in equation (1) is known only with considerable (in most cases) uncertainty because of disparate sampling densities, poor political or economic support, or inability to make an accurate measure. Estimation of **E**, and the storage change term, however, is particularly problematic. **E** is often estimated as the closure term, and over long-term averages, $d\mathbf{S}/dt$ is often ignored. However, the latter approach precludes consideration of surface water dynamics, and even over long times, storage change can be important. For example, despite a slight increase in Arctic precipitation, Siberian lake area and numbers have decreased: a phenomenon recently identified by *Smith et al.* [2005], which they attribute to regional variations in the melting of permafrost. Increased Arctic river discharge has been linked to increased temperatures, particularly in the Arctic [*Peterson et al.*, 2002]. Lacking spatial measurements of wetland locations, sizes, and volumetric changes, hydrologic models are unable to properly represent the effects of surface storage on river discharge [e.g., *Alsdorf*, 2003]. Errors can exceed 100% because wetlands modulate runoff through temporary storage and change the dynamics of both runoff generation (through direct communication of precipitation with the expanded channel system) and evaporation [e.g., *Coe*, 2000].

[10] While global Earth system models continue to improve through incorporation of better soils, topography, land use and land cover maps, their representations of the surface water balance are still greatly in error in large part because of the absence of a coherent observational basis for quantifying river discharge and surface water storage globally. Thus open questions such as the following remain relative to the land surface water budget: What is the spatial and temporal variability in the world's terrestrial surface water storage? In response to global warming, how are freshwater volumes changing throughout the Arctic and elsewhere? What have been the effects of reservoir construction and diversions of surface water on the dynamics of the land surface water budget globally?

### 3.2. Flow Hydraulics

[11] Floodplains are marked by a rich variety of water sources including over-bank flows (regional contributions) as well as groundwater, hyporheic water (the saturated zone under a river), local tributary water, and direct precipitation (local contributions) [*Mertes*, 1997]. Floodplain flow is equally complex and includes diffusive transport across broad, flat pans, temporary storage in lakes of varying morphologies, and slow drainage through a maze of channels of various widths, depths, degrees of boundary definition, and vegetation densities (Figure 1). This complexity impacts water balance and wetland ecologies. For example, on the basis of Muskingum modeling (a continuity-based water storage and transport method), *Richey et al.* [1989] estimate that the main Amazon River alone exchanges about 25% of its average annual flow with its adjacent floodplain. Although this percentage is greater than twice the discharge of the Mississippi River, the estimate is not constrained by any in situ floodplain gauges (no gauges are installed on the floodplain). In fact, *Alsdorf* [2003] used spaceborne synthetic aperture radar (SAR) measurements of the floodplain to demonstrate the possibility of significant errors in this estimate. Given that the Amazon Basin contains about 750,000 $km^2$ of annually inundated area [*Melack and Forsberg*, 2001], the impacts likely extend far beyond the main stem.

[12] Similarly, the flow of water through braided rivers is difficult to measure from gauges because braided rivers contain dynamic channels that increase in number, widen, and shift in response to changes in discharge (Figure 2). Arid, glacierized, and high-latitude basins all typically contain braided rivers, yet their geomorphic complexity limits in situ efforts to measure flow variations related to

**Figure 2.** Arctic braided river. Braided rivers frequently shift channels during floods; thus the reinstallation of gauges and related bathymetric surveys can frequently be required when using in situ methods to estimate discharge. Photograph courtesy of K. Douce.

the climatically induced retreat of many of the world's alpine glaciers [e.g., *Thompson et al.*, 2000]. The remote location of Arctic river basins has led to a sparse (and declining, especially since the collapse of the former Soviet Union) gauging network in the Arctic despite the importance of the Arctic freshwater discharge to global climate.

[13] Unfortunately, nearly all of the world's wetlands lack in situ measurements of dynamic extent, storage, and flow, while the remoteness and morphology of many Arctic braided rivers limits gauging methods. Consistent and accurate spaceborne measurements of floodplain and braided river hydraulics would allow key hydrologic questions such as the following to be answered: How much water is stored on a floodplain and subsequently exchanged with its main channel? What are the local and continental-scale responses of braided rivers to climate-induced changes in glacier mass balances?

### 3.3. Global Health, Flood Hazards, Water Resources, and Management

[14] The impact of water availability on humankind is obviously great. Thousands of people perish each year because of floods, whereas over 2 billion lack adequate drinking water or sanitation [*Gleick*, 2003]. Indeed, population growth by 2025 is expected to impact water availability more significantly than the impacts of greenhouse warming on water systems [*Vörösmarty et al.*, 2000]. Major health issues are also tied to fresh water. Disease vectors such as malaria are a function of mosquito habitats, which, in turn, are directly related to water surface areas. Yet there currently is no basis for mapping the spatial and temporal variability in these highly dynamic and sometimes intermittent water bodies. Thus, while water resource issues will have large effects on many of the world's major decisions in the coming decades, the absence of coherent observations of surface water storage changes and fluxes will limit predictive capabilities regarding future water availabilities and related health issues.

[15] Land use changes on both the floodplain and in surrounding upland catchments have altered naturally occurring flood hydrographs. Examples include the direct encroachment of urbanized areas upon the floodplain and conversions from forest to pasture in surrounding basins. The patterns and extents of floods directly impact the economies, lives, and health of communities within flooded areas. For example, floodplains contain fertile soils for agriculture, but deposition of sediment and erosion of topsoil during flooding can destroy farmlands resulting in billions of dollars in losses (e.g., Mississippi River flooding of 1993 [*Jacobson and Oberg*, 1997; *Vance*, 1994]). Predictions of flood hydrographs have largely been limited to statistical (e.g., flood frequency analyses [*Stedinger et al.*, 1993]), physically based (e.g., incorporation of catchment response [*Robinson and Sivapalan*, 1997]), and one-dimensional in-channel models for flood routing [e.g., *Moussa and Bocquillon*, 1996]. Yet these methods do not predict the area of inundation. Inundation hydraulics must account for the varied water sources (section 3.2) as well as the interaction of the flow with floodplain topography,

**TABLE 1. Satellites and Available Data for Surface Water Measurements**

| Space Agencies and Satellites | Online Data Location |
|---|---|
| WATER mission concept | |
| U.S. WATER | earthsciences.osu.edu/water |
| Response to National Research Council | http://www.nap.edu/catalog/11820.html |
| European Union WATER | www.legos.obs-mip.fr/recherches/missions/water/ |
| Japan Aerospace Exploration Agency L band SAR missions | |
| JERS-1 | www.eorc.jaxa.jp/JERS-1 |
| ALOS phased array type L band synthetic aperture radar (PALSAR) | www.jaxa.jp/missions/projects/sat/eos/alos/index_e.html |
| Global Rain Forest Mapping | www.eorc.jaxa.jp/JERS-1/GFMP |
| European Space Agency (ESA) C band ERS-1 and ERS-2 SAR missions | earth.esa.int/ers |
| NASA–Centre National d'Etudes Spatiales (CNES) TOPEX/Poseidon and Jason-1 radar altimeters | |
| NASA TOPEX/Poseidon | sealevel.jpl.nasa.gov/mission/topex.html |
| NASA Jason-1 | sealevel.jpl.nasa.gov/mission/jason-1.html |
| CNES TOPEX/Poseidon | www.cnes.fr/html/_455_461_1461_.php |
| CNES Jason-1 | www.cnes.fr/html/_455_461_1441_.php |
| ESA ERS-1 and ERS-2 radar altimeters | earth.esa.int/ers/ra |
| NASA–Deutschen Zentrum für Luft- und Raumfahrt (German Aerospace Center)–U. S. Geological Survey (USGS) SRTM | |
| NASA mission | www.jpl.nasa.gov/srtm |
| DLR mission | http://www.dlr.de/srtm/ |
| USGS data archive | srtm.usgs.gov |
| NASA–Center for Space Research (University of Texas) ICESat | |
| NASA Goddard Space Flight Center | icesat.gsfc.nasa.gov |
| CSR | www.csr.utexas.edu/glas |
| Surface water remote sensing groups | |
| NASA Surface Water Working Group | earthsciences.osu.edu/swwg |
| Laboratoire d'Etudes en Géophysique et Océanographie Spatiales–CNES hydrology from space | gos.legos.free.fr |
| Surface water altimetry data | |
| U.S. Department of Agriculture–NASA–University of Maryland | www.pecad.fas.usda.gov/cropexplorer/global_reservoir/index.cfm |
| ESA River and Lake Program | earth.esa.int/riverandlake |
| LEGOS-CNES Program | www.legos.obs-mip.fr/soa/hydrologie/hydroweb/ |

vegetation, and standing water. With the advent of faster computers, recent attempts have been made to predict the area of inundation and depth of flow using two-dimensional finite element models of shallow water flow [e.g., *Horritt*, 2000; *Bates et al.*, 1997]. Unfortunately, verification and calibration of the models suffer greatly from a lack of coincident floodplain water height and inundation extent observations during extreme flooding.

[16] Many of the Earth's major rivers cross international boundaries, which confuse decision processes regarding river management. In many such cases, information regarding water storage, discharge, and diversions in one country that affect the availability of water in downstream neighbors is not freely available (examples include the Nile, Indus, Mekong, Tigris, and Euphrates rivers). In fact, hydrological observations that have implications for water management often are closely guarded and are only released, if ever, many years after any practical utility has passed. As an example the Southeastern Anatolia Project (GAP) (see www.gap.gov.tr) in Turkey was initiated in 1976 with the goal of constructing 22 dams and 19 hydroelectric plants on the Tigris and Euphrates rivers, effectively controlling nearly all of the discharge of those rivers to downstream Syria and Iraq (presently, about 40% of the project is complete (F. Schwartz personal communication, 2005)). Spaceborne measurements of reservoir storage globally would ensure a free and open exchange of data necessary for water management, unconstrained by international boundaries.

[17] Lacking global and consistent measurements of water storage and discharge, questions such as the following remain: How do water surface elevations vary across floodplains in urbanized and natural environments, and what are the corresponding extents of inundation? What are the policy implications of freely available water storage data for water management? Can health issues related to waterborne diseases be predicted through better mapping of surface water extent?

## 4. MEASUREMENTS REQUIRED TO ADDRESS SCIENCE AND APPLICATIONS THEMES

[18] *Alsdorf and Lettenmaier* [2003] have considered the questions posed in section 3 and determined that answering them will require approaches that fundamentally differ from in situ, gauge-based methodologies that are currently

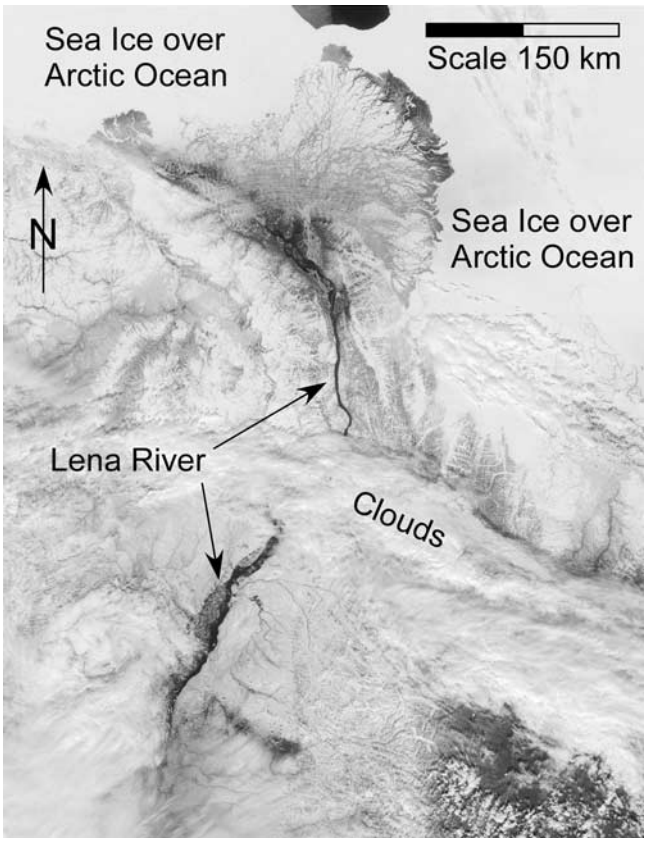


**Figure 3.** Lena River and delta, Siberia [*Alsdorf et al.*, 2003]. This 500 km × 650 km Moderate-Resolution Imaging Spectroradiometer image with 250-m pixels from June 2002 illustrates a small portion of the vast, seasonally snow-covered Arctic area available for snowmelt runoff and the difficulty in using optical wavelengths to image beneath clouds (note the disappearance of the Lena River beneath the clouds). NASA image from visibleearth.nasa.gov.

the norm. Hydraulic measurements that are central to the fluid equations of motion include elevations of the water surface ($h$), temporal changes in water levels ($\partial h/\partial t$), water surface slope ($\partial h/\partial x$), and inundated area. Essentially, temporally repeated measurements of $h$ provide a basis for estimating $\partial h/\partial t$, which summed over an inundated area is a measure of the volume of water lost or gained during a time interval. Water storage is a key variable in continuity-based estimates of mass balance, whereas $h$ is a state variable in hydrodynamic models that predict flow hydraulics through channels and wetlands.

[19] Neither in situ nor remote sensing methods measure discharge; rather, it is a derived quantity. Because discharge represents flux through a channel cross-sectional area, the combination of the depth-integrated velocity profile and channel bathymetry is required for traditional in situ discharge estimates. As discussed in section 5.6, spaceborne approaches to acquiring such measurements are likely to remain elusive because of the inability of today's electromagnetic sensors to routinely penetrate into water bodies to sufficient depths. Instead, data assimilation schemes that use the hydraulic measurements noted above are more likely to provide near-term solutions to estimating discharge from space (section 6.4).

## 5. SUMMARY OF EXISTING SPACEBORNE METHODS FOR MEASURING SURFACE WATERS

[20] In this section we summarize previous satellite-based methods of characterizing surface water hydraulics. We also highlight the successes and limitations of the methods. The goal of this section is to show the sampling possibilities from existing sensors (Table 1) and to demonstrate the related potential for estimation of hydrologic variables (section 4) toward answering the questions of section 3.

### 5.1. Methods for Measuring Area

[21] Surface water extent can be measured with a variety of visible band sensors (e.g., Landsat, Moderate-Resolution Imaging Spectroradiometer (MODIS), and SPOT) with different repeat frequencies and by SAR imagery (e.g., RADARSAT, JERS-1, and ERS) [e.g., *Smith*, 1997; *Brakenridge et al.*, 2005; *Mertes*, 2002; *Papa et al.*, 2006; *Prigent et al.*, 2001]. Such approaches have met with some success, but their routine application can be limited. Problems with visible band sensors include cloud cover, as well as modest spatial resolution for sensors with short repeat intervals, such as MODIS (Figure 3). Estimation of surface water extent in the Amazon is further compounded by smoke from forest fires. Optical sensors also fail to image the water surface beneath flooded vegetation canopies, a significant problem in the Amazon where about 70% of the floodplain is marked by inundated forests [*Mertes et al.*, 1995]. Other tropical basins, such as the Congo, have similar vegetation coverage [*Mayaux et al.*, 2002]. SAR-based estimates of surface water extent are confounded by difficulties with wind roughening of the water surface for the wavelengths used by most existing sensors (Figure 4, e.g., the 5.7-cm C band wavelengths of ERS-1 and ERS-2 [*Smith and Alsdorf*, 1998]). Multitemporal interferometric SAR coherence can be used to delineate inundated surface area because the scattering characteristics of water surfaces continually change with waves, resulting in poor repeat-pass coherence over water [*Smith and Alsdorf*, 1998]. This approach, however, requires the temporal coherence of the surrounding land surface to remain relatively greater, a condition not typically met for orbital repeat cycles greater than a few days (snow, rain, and wind between acquisitions alter dielectric properties of surrounding land and vegetation surfaces, resulting in poor coherence everywhere).

[22] Perhaps the best opportunity in the next few years for routine measurements of inundated area will result from the Japan Aerospace Exploration Agency's ALOS mission (the primary payload of the Advanced Land Observing Satellite is a 24-cm wavelength L band SAR system launched on 24 January 2006). At longer L band wavelengths, radar energy can be reflected specularly because wind or wave action on terrestrial water surfaces is often insufficient to produce scattering energy back to the antenna

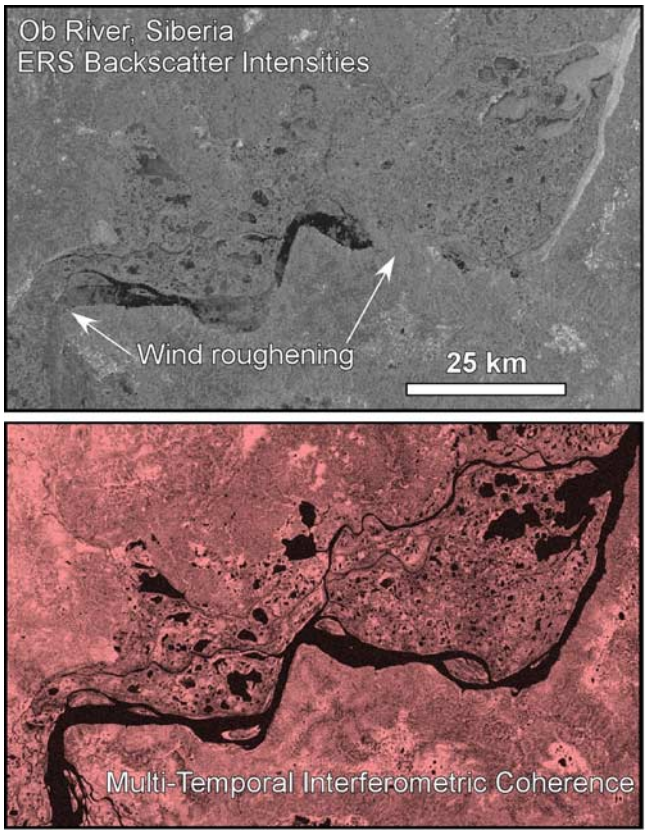


**Figure 4.** Synthetic aperture radar (SAR) C band (5.6-cm wavelength) imagery of the Ob River, Siberia. Although radar penetrates clouds, (top) the ERS SAR amplitude image shows that wind-induced waves on the river increase scattering. (bottom) The 1-day temporal baseline of the ERS-1 and ERS-2 tandem mission permits construction of interferometric coherence that delineates water from land surfaces [*Smith and Alsdorf*, 1998].

(in contrast, note that open ocean conditions often develop Bragg waves capable of backscatter to the antenna [*Alpers*, 1985]). Thus L band SAR backscatter data show low energy returns over open water surfaces (Figure 5). L band is also capable of penetrating vegetation canopies; thus, unlike all other typical sensors and wavelengths, it can routinely image the underlying flood water surface. The Global Rain Forest Mapping (GRFM) [*Rosenqvist et al.*, 2002] mission has produced continental-scale mosaics of inundated area throughout the tropical regions from L band SAR data collected by the Japanese Earth Resources Satellite (JERS-1). These mosaics are limited only by the acquisition times rather than by vegetative or weather conditions. The recently launched ALOS mission is scheduled for a number of seasonal acquisitions of global wetland areas.

### 5.2. Methods for Measuring Elevations

[23] Both profiling and imaging methods can be used for measuring surface water elevations from space. Radar altimetry methods are unquestionably the most successful given their long history with oceanographic applications.

#### 5.2.1. Elevations From Profiling Altimetry Methods

[24] Oceanic surface elevations have been routinely measured since the early 1990s using radar altimetry onboard the TOPEX/Poseidon (T/P) and ERS satellites and more recently from the Envisat and Jason-1 missions. The launch of the Ice, Cloud and land Elevation satellite (ICESat) in early 2003 has now made spaceborne lidar altimetry available for terrestrial water bodies. T/P and Jason-1 both include dual-frequency altimeters operating at Ku and C bands (2.2 cm and 5.6 cm wavelengths, respectively). Height resolutions of radar altimetry over river surfaces are ~10 cm at best and are more typically ~50 cm (e.g., Figure 6), but with increased averaging over large lakes (>100 $km^2$), accuracies improve to 3–4 cm RMS [e.g., *Birkett et al.*, 2002; *Birkett 1995*, 1998; *Maheu et al.*, 2003; *Hwang et al.*, 2005; *Frappart et al.*, 2006; *Cretaux et al.*, 2005; *Kouraev et al.*, 2004; *Birkett and Doorn*, 2004;

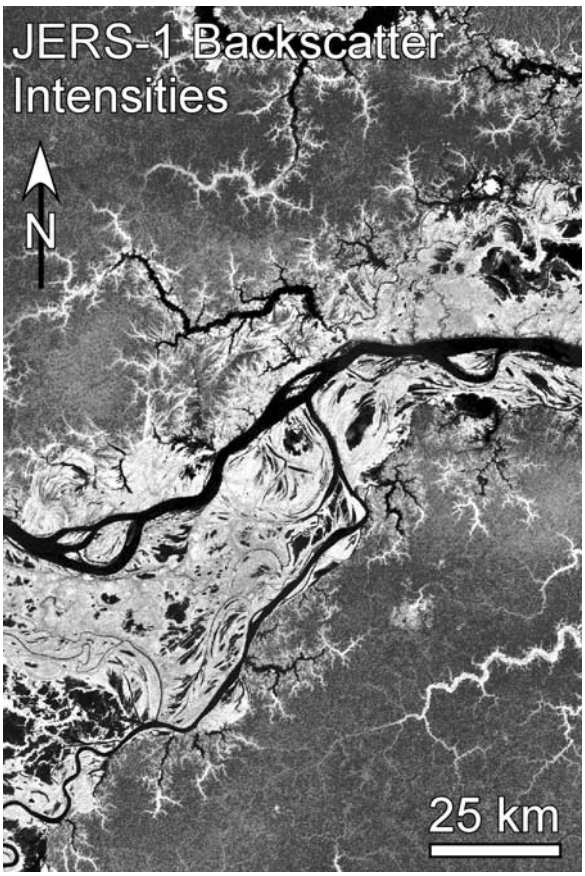


**Figure 5.** Confluence of the Solimoes and Purus rivers, Amazon Basin. These L band (24-cm wavelength) SAR data from the JERS-1 mission show low radar returns over open channels, intermediate amplitudes over dry land, and strong returns over inundated vegetation (i.e., in the floodplain). Typically, L band radar reflects specularly away from the antenna despite wind or wave action on the water surface of rivers, lakes, and wetlands. Radar energy will return to the side-looking antenna only when it interacts with the trunks of inundated vegetation (''double-bounce'' travel path). SAR data from Global Rain Forest Mapping high-water mosaic of May and June 1996 [*Rosenqvist et al.*, 2002] are shown.

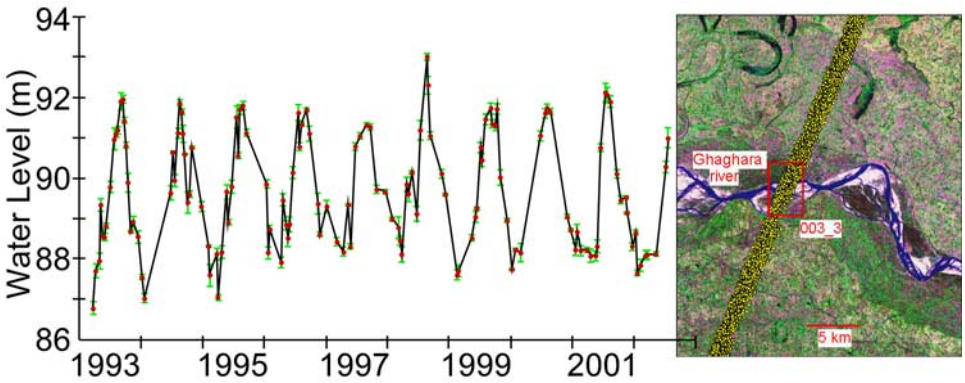


**Figure 6.** Water surface elevations of the Ghaghara River, India (82.17E, 26.82N), a tributary of the Ganges River. (left) TOPEX/Poseidon radar altimetry measurements (red dots) are collected only from (right) returns within the red box (yellow pixels measuring 580 m, Landsat image). Careful data selection is used to ensure measurements are from water surfaces. Error bars are 25 cm on average (minimum is 1 cm, maximum is 57 cm). For data see M.-C. Gennero et al. (Surface water monitoring by satellite altimetry, 2005, available at http://www.legos.obs-mip.fr/en/soa/hydrologie/hydroweb/).

European Space Agency, River and Lake Altimeter Data Sets for Surface Water Measurements, 2005, available at earth.esa.int/riverandlake; M.-C. Gennero et al., Surface water monitoring by satellite altimetry, 2005, available at http://www.legos.obs-mip.fr/en/soa/hydrologie/hydroweb/]. Note that compared to typical oceanic applications, inland water measurements from radar altimetry have a much degraded resolution because of reduced pulse averaging and differing echo shapes. Because presently operating radar altimeters do not take advantage of coherent Doppler processing (i.e., SAR-like processing), their spatial resolutions are on the order of kilometers instead of the <100-m sizes that are potentially resolvable (depending on microwave frequency).

[25] Spaceborne lidar, such as the Geoscience Laser Altimeter System (GLAS) instrument onboard ICESat, demonstrates height accuracies of 3 cm over a footprint of 70 m [e.g., *Schutz et al.*, 2005; *Harding and Jasinski*, 2004]. Pointing control is known to within 50 m, and despite the specular nature of water surfaces, up to 5° off-nadir measurements are possible. Subcanopy lidar elevation measurements result from penetration through vegetation openings, and similarly, thin to moderate cloud cover permits Earth surface measurements. The success of airborne lidar for water surface elevation measurements has not been similarly experienced in space. Limitations include the need for frequent pulsing to ensure along-track coverage given the typical 7 km/s velocities of spacecraft, which far outpace their airborne counterparts. An additional problem with lidar instruments is that they have no imaging capabilities, and it is not always clear whether a return is due to land or water surface without additional information, such as observation of an extended flat surface, when large water bodies are present. This problem is compounded for spaceborne lidar observations of small rivers: In this case the lidar footprint may be comparable in size to the width of the river (e.g., 70 m for ICESat's GLAS), and simultaneous returns from water and land are inevitable. The removal of the bank or vegetation contamination for the smaller water bodies and the identification of water and land returns remain subjects for research.

[26] It is important to note that all altimeters are profiling instruments and do not yield a two-dimensional image. Thus they essentially provide only spot measurements of water surface elevations with the exception of the rare case where the orbital track is subparallel to an elongated water body. Radar altimeters can be enhanced for imaging and height determination by using a slightly off-nadir imaging concept (discussed in section 6.5); however, a similar conversion is not possible with lidar. Rather, multiple lidar beams are required with each beam responsible for one pixel in the resulting image, or a helical scanning mode is required to essentially fill an area with lidar pulses from a single instrument.

### 5.2.2. Elevations From Imaging Methods

[27] Only the Shuttle Radar Topography Mission (SRTM) [*Farr et al.*, 2007] has produced spaceborne, image-based elevation measurements of water surfaces (Figure 7). Because the SRTM C band system operated at 30°–60° look angles and the X band system operated at ~50° angles, radar pulse returns from water surfaces are a function of roughening by wind or wave action. As noted in section 5.1, shorter wavelengths generally produce greater backscatter than longer wavelengths for water surfaces in the off-nadir direction. For example, comparisons of the river channel and lake water surfaces in Figure 7 demonstrate that X band elevations are available everywhere, whereas portions of the C band digital elevation model (DEM) are missing surface elevation ($h$) values over water. At ±5.51 m (range of 3.69–8.25 m) for C band and ±18.8 m (range of 4.84–40.5 m) for X band the elevation accuracies over water surfaces are degraded compared to the surrounding terrestrial areas and compared to TOPEX/Poseidon measurements (statistics are from the Amazon River [*LeFavour and Alsdorf*, 2005] and from three reservoirs and the Muskingum River in the state of Ohio [*Kiel et al.*, 2006]).

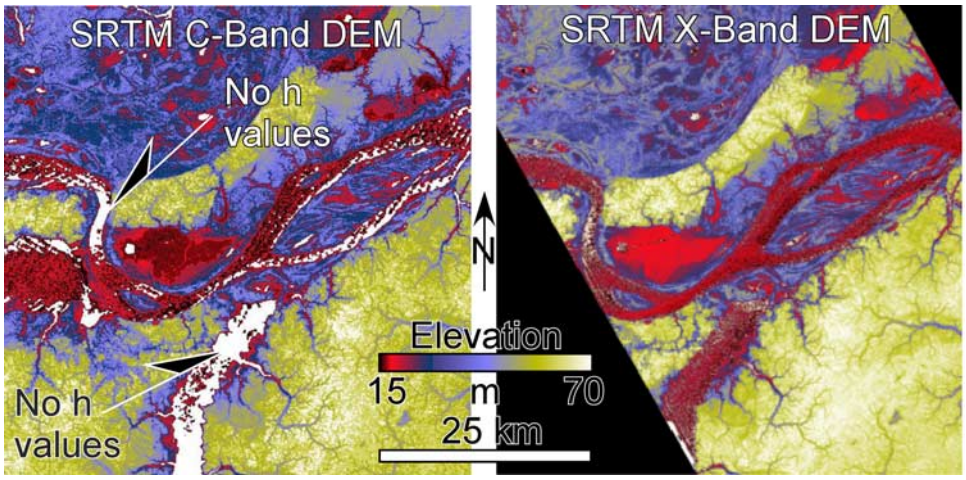


**Figure 7.** SRTM water surface elevations, $h$, on the Amazon River at Itapeua. Compared to X band, C band elevations are missing for significant portions of the channel and lake areas. Elevation accuracies over water surfaces in both digital elevation models (DEMs) are degraded compared to surrounding land (see *Kiel et al.* [2006] for explanation of degradation).

[28] Some efforts have used image-based measurements of inundated area overlain on a DEM to estimate shoreline elevations [*Brakenridge et al.*, 2005]. Although this approach does not provide a direct measurement of the water surface, it serves as a proxy measurement with a height accuracy related to the following factors: (1) The height accuracy of the DEM, in part, determines $h$; however, the global applicability of such an approach depends on the availability of a high-resolution DEM. Only the SRTM DEM provides a global source, but its relative vertical accuracy is 4.7–9.8 m (accuracy varies with each continent [*Rodríguez et al.*, 2006]). To use this SRTM-based approach to estimate $\partial h/\partial x$ for low-gradient rivers (i.e., 1.0 cm/km, section 4) requires multiple reach lengths of hundreds of kilometers to ensure that enough shoreline length is averaged to improve the $\partial h$ accuracy [*LeFavour and Alsdorf*, 2005] (section 5.4). (2) The accuracy of $h$ is also determined by the image resolution and the slope of the shoreline bathymetry wherein steep-sided channels or low-resolution imagery yield a poorer accuracy than gently dipping bathymetries and high-resolution images. For example, the Amazon Basin contains 750,000 km$^2$ of annually flooded area, thus using a typical satellite image size of 100 $\times$ 100 km to measure a small fraction of the inundation and using a reasonable 7 cm/d change in water levels over an 8-day period yields a flux of about 8000 m$^3$/s. Yet the 56 cm of $\partial h/\partial t$ is nearly undetectable given the SRTM DEM accuracy (the only DEM available for the Amazon), and the change in flooded area is almost undetectable at even the highest spatially resolved imagery. Unfortunately, this 8000 m$^3$/s error is large, about half the long-term average discharge of the Mississippi River. The problem is greatly exacerbated when considering the entirety of the Amazon wetlands. (3) DEMs often estimate an envelope of vegetation heights rather than the true subcanopy topography (e.g., the SRTM DEM, airborne lidar-based DEMs, and photogrammetry-based DEMs); thus the method can be subjected to great errors, especially for vast, lowland rivers that are blanketed with vegetation that often exceeds regional topographic highs. (4) Perhaps the single greatest factor affecting the accuracy of $h$ using this method is that it assumes that water levels between the shorelines are planar and without undulations (i.e., assumes a "bathtub" hydrology). This assumption may or may not be valid for river channels, but it is in error for floodplains (see section 5.3 and Figure 8).

### 5.3. Methods for Measuring Temporal Variations

[29] Temporal changes in water levels can be easily derived from repeated altimeter measurements (e.g., Figure 6), whereas repeat-pass interferometric SAR has recently provided an intrinsic, image-based direct measurement of $\partial h/\partial t$ [*Alsdorf et al.*, 2000; 2001a, 2001b; *Lu et al.*, 2005; *Kim et al.*, 2005]. The $\partial h$ accuracy of the method is centimetric. As noted in Figure 5, L band radar energy penetrates canopy and specularly reflects from the underlying water surface; thus the off-nadir method requires a radar pulse travel path that uses vegetation to return the echo to the antenna. Such inundated vegetation environments are plentiful throughout the Amazon wetlands but are not a global phenomenon. The method's greatest limitation is that it will not work over open water, i.e., typical river channels, lakes, and reservoirs.

[30] Figure 8 demonstrates the important, and previously unknown, hydraulics that occurs across floodplains, particularly during inundation [*Alsdorf*, 2004]. Many floodplain channels are conspicuous because $\partial h/\partial t$ changes are not equivalent on both sides, suggesting that flow delivery and decantation to surrounding floodplain areas is uneven. For example, some floodplain channels show that $\partial h/\partial t$ is greatest on the upstream side of the adjacent main channel during inundation (midrising $\partial h/\partial t$ surface, Figure 8 left topmost arrow), but at peak stage, water delivery from the Amazon River dominates, resulting in a greater $\partial h/\partial t$ on the downstream side of these floodplain channels. However, other floodplain channels, particularly those at a greater

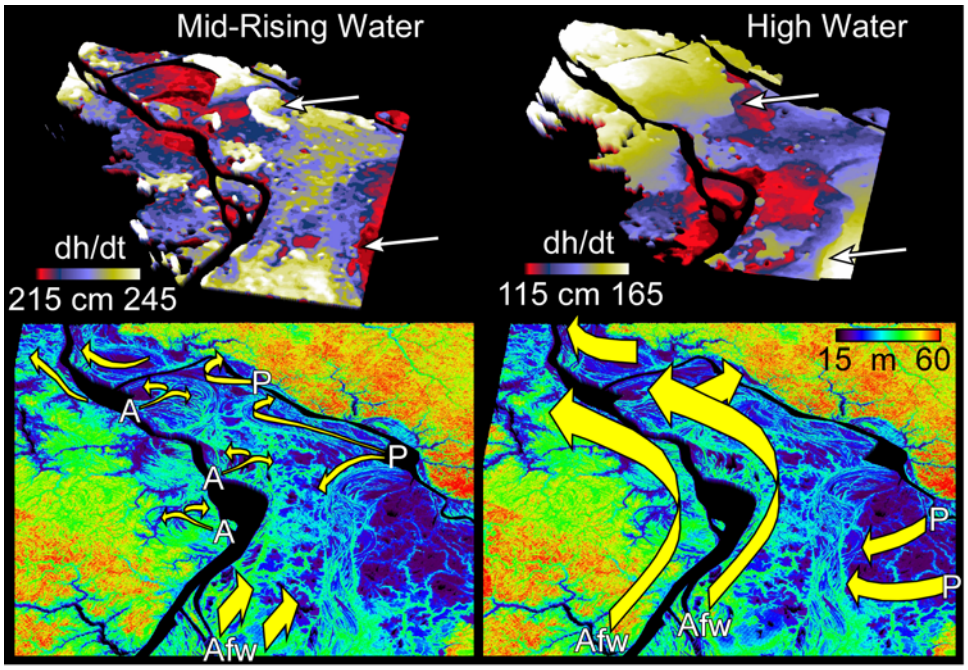


**Figure 8.** (top) Changes in water levels ($\partial h/\partial t$) and (bottom) perspective views of central Amazon floodplain topography. View is looking east, and panels are 75 km across the foreground. Colors indicate water level rise from (top left) 26 February to 11 April 1993 and (top right) 15 April to 12 July 1996. The top panels are entirely water surfaces (no land surfaces are plotted) and are measured from interferometric JERS-1 SAR phase. Sharp variations in $\partial h/\partial t$ occur across floodplain channels (arrows, top). These unexpected variations are indicative of flows and their transported sediments and carbon [*Alsdorf*, 2004]. A basic, continuity-based hydraulic interpretation suggests flow from low $\partial h/\partial t$ to high $\partial h/\partial t$; thus early and midrising water conditions are marked by (bottom left) local floodplain infilling followed by (bottom right) high-water conditions when the large flood wave moves subparallel to the main Amazon channel. P indicates water from the Purus River; A denotes water from the Amazon River; and Afw is the Amazon flood wave.

distance from the Amazon River, show the opposite trend. A preliminary hydraulic interpretation suggests that during the rising limb of the hydrograph, inundation appears first as a patchwork bordered by small floodplain channels, whereas at main stem peak stage, floodplain flow appears to be subparallel to the main stem Amazon. Essentially, the hydraulics of Amazon floodplain inundation is a complex interaction of local geomorphology and water stage. These views are only apparent from a spaceborne platform, yet they are key for improving our understanding of floods and their transported biogeochemical and sediment constituents.

[31] Note that at the ~25° and greater incidence angles used by most SAR antennae, C band energy does not penetrate vegetation canopies in a manner similar to longer L band wavelengths. For example, *Alsdorf et al.* [2000, 2001a] found poor temporal coherence from interferometric Spaceborne Imaging Radar C band data over the heavily forested Amazon floodplain. However, recent work by *Lu et al.* [2005] has demonstrated that interferometric ERS-1 and ERS-2 SAR data contain reliable temporal phase coherence over the moderately forested swamps of southeastern Louisiana. More work is needed to further clarify the potential use of the abundant C band data archives, but the preliminary assessment is that radar wavelengths shorter than L band and at significant off-nadir incidence angles can penetrate some canopies and thus provide a useful $\partial h/\partial t$ measurement.

### 5.4. Methods for Measuring Slope

[32] Rather than an intrinsic measurement, water slopes are derived from elevation measurements collected by altimeters or by SRTM. Altimetric methods use the distance between orbits with the measured $h$ values to calculate $\partial h/\partial x$; thus there is an inherent time lag between $h$ acquisitions that is built into the slope calculation [e.g., *Birkett et al.*, 2002]. For gradually developing flood waves, such as the Amazon, such temporal discontinuities are minor. Because of the degraded height accuracy, slopes calculated from SRTM require reach lengths suitable for decreasing the noise. For example, in Figure 9 a polynomial is fitted to the extracted $h$ values along most of the main stem Amazon River, which allows a simple derivative calculation [*LeFavour and Alsdorf*, 2005]. These SRTM-derived slopes also contain some temporal averaging related to the acquisitions over the 11 days of the shuttle mission, but the expected change in slope during the mission was only about 0.02 cm/km, compared to the 2–3 cm/km slopes measured. These $\partial h/\partial x$ values compare well to ground truth and to T/P measurements.

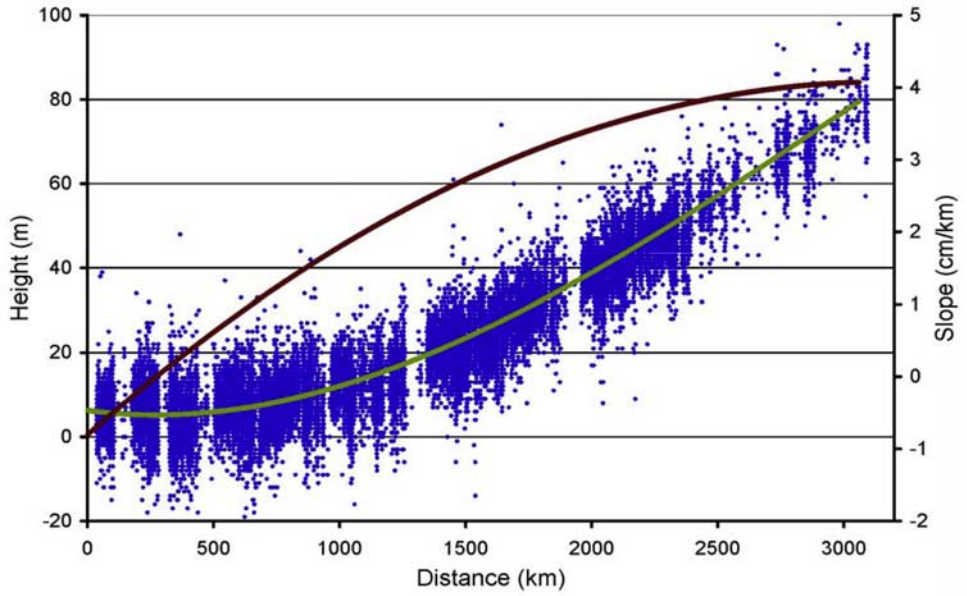


**Figure 9.** Estimated elevation (green line) and slope (red line) of the Amazon River. A third-order polynomial (green line) fitted to water surface SRTM elevations (blue dots) from the main Amazon channel provides a derivative for estimating slope variations along the entire profile [*LeFavour and Alsdorf*, 2005].

### 5.5. Methods for Measuring Velocity and Estimating Discharge

[33] Noncontact methods are being developed to measure surface water velocity and to estimate discharge. An intriguing new contribution uses ground-penetrating radar to define the channel cross section and pulsed Doppler radar to measure surface velocity: Combined, the observations yield discharge [*Costa et al.*, 2000, 2006]. Presently, this approach is based on bank side or airborne observations but does not provide a synoptic view necessary for large floodplains; therefore it is not apparent how it can be transferred to satellites. Preliminary research based upon airborne Doppler lidar wind measurements has been explored for rivers and other water bodies as targets for velocity measurements [*Emmitt and Kavaya*, 2001], but much more work is required to evaluate the capabilities. Interferometric processing of two airborne SAR antennae aligned in an along-track orientation is an image-based method for producing surface velocities and has been well documented for nearshore oceanic environments [e.g., *Goldstein et al.*, 1989; *Goldstein and Zebker*, 1987]. Application of this airborne method to riverine environments is much less documented, but some recent successes show promise for deriving one component of the velocity vector [e.g., *Bjerklie et al.*, 2005].

[34] The only spaceborne measurement of river velocity has been derived from interferometric processing of SRTM's X band SAR data [*Romeiser et al.*, 2005]. The approach of Romeiser et al. relies on the short along-track offset of 7 m between the two X band antennae, a useful coincidence due to SRTM's payload configuration. The accuracy of the method is limited by this short offset and the ~7.5-km/s shuttle velocity. For river water velocities less than 1 m/s, a reach length of at least 1 km is required for spatial averaging to reduce random errors.

[35] The problems with measuring velocities are significant. Because of the sharp dielectric contrast between air and water, typical optical or microwave spaceborne technology will not routinely penetrate the water surface sufficiently to provide a velocity profile (see discussion in section 5.6). Thus methods are confined to measuring velocities across the water surface not the subsurface velocity profile that hydrologists use at gauging stations to estimate discharge. The velocities measured by this technique are those of Bragg waves [*Alpers*, 1985], induced by wind forcing and river turbulence, which have a characteristic intrinsic velocity and are further advected by the river velocity [*Plant et al.*, 2005]. Since there is no guarantee that wind forcing occurs along the direction of water flow, the measured velocity can have a significant cross-channel component, which is not indicative of the integrated downstream velocity. Successful estimation of the downstream flow has been done for in situ radar systems by measuring the velocity from multiple directions, a technique which is not easily implemented from space. Calibration of the Bragg component can be attempted by using the assumption that the river bank does not move, but, as noted by *Plant et al.* [2005], it is required that the river bank topography be known to high accuracy, which, in general, is not possible. A fundamental problem will always exist when wind-induced velocities differ from the true current direction or overly amplify the velocity magnitude. This is a significant issue for floodplains where flows are small compared to the main channel and where localized wind forcing may suggest flows not representative of the flow at depth. Furthermore, spaceborne methods will likely

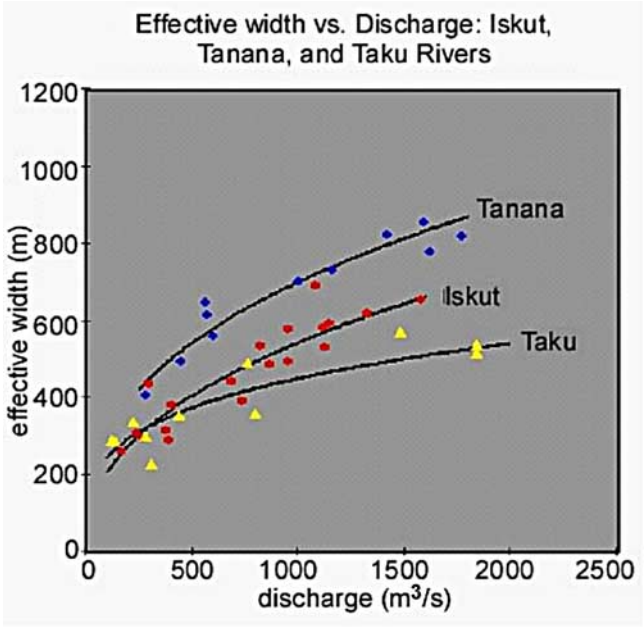


**Figure 10.** In situ discharge correlated with remotely sensed inundated area. "Effective width" determined from SAR imagery is a measure of the inundated area during flood events for three braided rivers in the Arctic. Discharge was determined from a gauge at a downstream coalescing of channels. The three curves represent possible rating curves to predict discharge in the absence of gauge data [*Smith et al.*, 1996].

measure only the one component of the velocity vector lying in the look direction because of the difficulty of implementing spaceborne vector along-track interferometers. Errors in this approach increase when the look direction approaches perpendicularity with the true velocity vector.

[36] Several approaches have been proposed that measure inundated floodplain or channel areas and use these to estimate discharge. Active and passive microwave sensors have been successfully used to determine the area of inundation [*Sippel et al.*, 1998; *Hess et al.*, 1995], and provided that in-channel gauge data are available for regression analyses of area and discharge, the inundated area can be used with varying degrees of accuracy as a proxy for discharge [e.g., *Smith*, 1997; *Vörösmarty et al.*, 1996]. However, because of the very low spatial resolution of passive sensors this method does not separate floodplain storage changes from main channel discharge and does not work well in environments where small changes in water heights yield little change in surface area yet significant changes in flow (e.g., section 5.2.2).

[37] A more recent approach combines image-based shoreline estimates of water surface elevations (i.e., section 5.2.2) with image-based measurements of changes in channel width and places these parameters within various empirical, logarithmic functions that relate discharge to hydraulic measurements [*Bjerklie et al.*, 2003; *Brakenridge et al.*, 2005]. Logarithmic expressions are well established for in-channel flows [*Leopold and Maddock*, 1953; *Leopold et al.*, 1964]. Unfortunately, they are generally not applicable to over-bank flows because the wetted perimeter and velocity profiles change significantly when moving from channel to floodplain [e.g., *Leopold et al.*, 1964]. *Leopold et al.* [1964, page 218] further caution that "[in a study of] ... the geographic distribution of values of the exponents ... over the United States ... clear-cut patterns do not exist ..." because rivers express increased discharge by widening channels in easily eroded banks or deepening where bank materials are cohesive (the exponents describe the logarithmic functions). For example, for reach lengths of over 100 km, water in the Amazon River channel widens by ~1% yet deepens by ~33% while the discharge increase is easily 100%, essentially negating width as an important indicator of in-channel discharge (width is still an important indicator of channel geometry). Given the cautions indicated in section 5.2.2, the imaged shoreline DEM method of estimating slopes is problematic, and in any event it is not globally applicable.

[38] Unlike single-channel rivers, which respond to increased discharge by depth increases (until bankfull stage), braided rivers with easily eroded banks respond by greatly increasing the width and number of channels. Therefore image-based approaches to estimating discharge or storage changes may be appropriate for some multichannel environments. *Smith et al.* [1995, 1996] have used SAR imagery to measure the area of flooded braided stream channels and reduced this area to a reach length "effective width" (Figure 10). Like a typical rating curve developed for well-defined channel cross sections and in-channel water heights, this width was shown to be correlated with in situ measurements of discharge, thus providing an image-based approach to estimating braided river discharge.

[39] Instead of using river width as a proxy for discharge, the advent of radar altimetry permits river water heights to be correlated with in situ estimated discharge [e.g., *Kouraev et al.*, 2004; *Zakharova et al.*, 2006]. Stream gauges are rarely located within the altimeter footprint but are typically within ~100 km; thus errors are related to differences in stream geomorphology between the in situ and satellite overpass locations. These methods are correlative, lacking rating curves and cross-sectional geometries; however, they do provide discharge estimates for times when in situ stage heights are missing.

[40] Fundamentally, all of these methods rely on in situ gauge data either to create regression curves or to train and select models. They are essentially empirical. The transferability of derived exponents for area-discharge relationships from one hydrogeomorphology to another is not proven.

[41] A recent advance on the above methods uses Muskingum-Cunge water balance modeling, constrained by channel surveys and in situ discharge, to derive stage-discharge relationships for altimeter overpass locations [*Leon et al.*, 2007]. The modeling helps constrain channel depths and results in derived bottom slopes in close agreement with altimeter-measured surface water slopes.

[42] A new effort to estimate discharge from mostly spaceborne data has been suggested by *LeFavour and Alsdorf* [2005]. They use the well-established Manning's equation [e.g., *Albertson and Simons*, 1964; *Leopold et al.*, 1964] for in-channel flows to estimate discharge at three locations on the Amazon River. Parameterization of Manning's equation uses $\partial h/\partial x$ from SRTM (Figure 9 and section 5.4), channel widths measured from GRFM SAR mosaics, depths from navigational charts, and a typical channel bed roughness value for Manning's $n$. Predicted discharges are within 8% or better of measured in situ values. This approach is promising because it relies on remotely sensed hydraulics rather than in situ measured discharge, but it is considered preliminary until more global locations are tested. The reliance on Manning's equation and navigational charts limits the method to in-channel flows on rivers with in situ measurements of depths (cross-sectional bathymetries on the Amazon were not required).

### 5.6. Methods for Measuring Bathymetry

[43] Airborne lidar has provided bathymetric maps of nearshore ocean environments to 40-m depths with accuracies of 15 cm for clear waters [e.g., *Wozencraft and Lillycrop*, 2002]. Depth penetration can be limited by turbidity, heavy surface waves, and Sun glint [e.g., *Banic and Cunningham*, 1998; *Davis*, 2004] such that, in practice, maximum detectable depths are no more than 2–3 times the Secchi depth [*Wozencraft and Lillycrop*, 2002]. Typical Secchi depths for the Ohio River main stem average 1.33 m and 0.52 cm on a tributary, the Muskingum [*Sanders*, 1992], whereas the channel depths are about 10 times these Secchi values. Thus the routine application of lidar to map channel bottoms is an active area of research.

[44] Knowledge of bathymetry is critical for calculating discharge; unfortunately, no spaceborne method exists that will routinely penetrate water to the necessary depths. Instead, channels and wetlands that occasionally drain with bottom exposures can be measured remotely and, assuming the bathymetry changes little, used to calculate discharge. This approach will not work for many rivers, such as the Mississippi, which never experience complete drainage. However, even in the absence of complete bottom exposure it may be possible to use repeated measurements of coincident surface elevation and width and to infer, via standard mathematical forms (e.g., power functions), the cross section of the unmeasured portion.

### 5.7. Methods for Measuring Mass

[45] The mass of water in the Earth system (atmosphere, surface, and subsurface), hence its volume, is being measured by the Gravity Recovery and Climate Experiment (GRACE) satellites [e.g., *Tapley et al.*, 2004; *Wahr et al.*, 2004; *Ramillien et al.*, 2005]. Because of the inverse distance squared relationship of gravity and mass, at an altitude of ~500 km the mission is only sensitive to basins larger than ~200,000 km$^2$ [*Rodell and Famiglietti*, 1999, 2001; *Wahr et al.*, 1998]. Data analyses methods are greatly improving on the spatial and temporal resolutions from the earliest GRACE data releases [*Han et al.*, 2005; *Schmidt et al.*, 2006], yet the space altitude will ultimately restrict the resolution. The derived month-to-month mass changes are a summation of all temporally varying components of the water column including precipitation, surface water, soil moisture, and groundwater (see equation (1)). This summation is essential for characterizing very broad patterns in terrestrial water storage such as those described in land surface models [e.g., *Ngo-Duc et al.*, 2007; *Swenson and Milly*, 2006] but will not, by itself, provide a basis for estimating flow hydraulics.

## 6. CHALLENGES FOR THE FUTURE OF SPACEBORNE APPROACHES TO MEASURING HYDRAULICS

[46] As presented in sections 6.1–6.4, by themselves, none of the technologies of section 5 supply the water volume and hydraulic measurements needed to model the water cycle accurately and to guide water management [*Alsdorf et al.*, 2003; *Alsdorf and Lettenmaier*, 2003]. Approaches for expanding the studies of section 5 to global observations include assimilation of the spatially and temporally disparate hydraulic measurements from multiple existing sensors or construction of a new sensor. Both approaches must be capable of providing measurements necessary for answering the key hydrologic questions of section 3.

### 6.1. Why Spaceborne Measurements Are Required

[47] As suggested in each of the three categories of questions (sections 3.1–3.3), existing in situ stream gauging networks are incapable of measuring the discharge and storage changes of wetlands and braided streams (section 2). Densification of these networks seems unlikely, especially given that most stream gauging networks globally are, instead, experiencing a decrease in station numbers [e.g., *Shiklomanov et al.*, 2002; *Stokstad*, 1999]. Nevertheless, spaceborne technological objectives should not include the replacement of measurements already collected by existing in-channel gauging networks or the replacement of lost measurements. Indeed, because of their higher accuracy, in situ point measurements of discharge are almost always preferred to remotely sensed measurements where specific, local objectives are involved. Instead, spaceborne measurement goals stem from the scientific questions (sections 3.1–3.3), which dictate a spatial measurement of hydraulics and basin-wide hydrologies.

[48] Two examples help to illustrate the problem. (1) The hydraulics and flow complexity demonstrated in the $\partial h/\partial t$ mapping in Figure 8 cannot be mapped with a single gauge or even a collection of gauges. This hydraulically dynamic flow regime transports sediments and biogeochemical fluxes into this two-river confluence and greatly enriches the ecology. However, without spatial measurements of $h$, $\partial h/\partial t$, and $\partial h/\partial x$ it remains essentially impossible to accurately predict the transport pathways of these important constituents. Furthermore, the potential damage related to

**Figure 11.** Arctic lakes. These lakes vary in size and have differing water level fluctuations [i.e., *Smith et al.*, 2005]. It is not possible to completely sample this distribution from a conventional altimeter (e.g., pulse limited in Figures 12–14). In situ gauging would require thousands of stations to monitor all lakes. A possible approach is the wide-swath interferometric altimeter discussed in section 6.5. Photograph courtesy of K. Frey.

pollutant spills from planned and existing infrastructure elements (e.g., oil pipelines and shipping vessels) cannot be tracked or predicted without spatial mappings of the flow hydraulics. (2) As another example, the surface water area of the Arctic is about 600,000 $km^2$ with countless lakes (Figure 11) of differing water levels in an overall wetland area of about 4.5 million $km^2$ (north of 45.5°N (L. C. Smith et al., A first pan-Arctic assessment of the influence of glaciation, permafrost and peatlands on northern lake distributions, submitted to *Permafrost Periglacial Processes,* 2006)). Satellite imaging of hydrologic fluctuations in nearly 10,000 Siberian lakes and wetlands has recently identified a previously unrecognized process of lake drainage triggered by climate warming and permafrost thaw currently underway in the Arctic [*Smith et al.*, 2005]. Essentially, some lakes are disappearing, whereas others remain (i.e., have differing $\partial h/\partial t$ rates), but with an overall increase in lake area in northernmost Arctic, while generally decreasing in the south. The lakes also release large quantities of water vapor, carbon dioxide, and methane to the atmosphere, absorb more solar energy than surrounding terrain, and can export large quantities of dissolved organic carbon from the land surface to oceans [*Frey and Smith*, 2005]. Economics, the remote Arctic location, and the difficulty of gauging thousands of Arctic lakes (Figure 11) greatly restrict in situ measurements, whereas spaceborne remote sensing remains viable.

### 6.2. Problems With Existing Sensors

[49] Problems with existing satellite-based technologies for measuring surface waters range from poor resolutions to inabilities to penetrate clouds or smoke. Poor spatial resolutions are associated with GRACE and all profiling altimeters. Conventional radar and lidar altimetry is nadir-viewing and misses water bodies between orbital tracks (details in section 6.3.1). Presently operating radar altimeters are not built to sample small freshwater bodies, compared to the surface of the open ocean; thus height and along-track resolutions are problematic. Although SRTM produced a high spatial resolution image of heights, the errors over water surfaces are quite large. Poor temporal resolutions are associated with SRTM, which operated for 11 days in February 2000, and with interferometric SAR, where repeat orbits are usually monthly, at best, leading to a prolonged $\partial t$ in the $\partial h/\partial t$ mapping. Repeat-pass interferometric SAR will not work over open water; instead, it requires special hydrogeomorphologies of flooded vegetation. Optical sensors cannot penetrate the canopy of inundated vegetation and typically fail to image water surfaces when clouds or smoke are present. Vegetation and atmospheric conditions prevalent in the tropics lead to performance degradation. However, it is important to recognize that the spatially or temporally local studies discussed in section 5 demonstrate the power of spaceborne measurements to enable hydrologists to move beyond the

point-based observations provided by gauge networks to a broader basin-wide space-time view.

### 6.3. Required Spatial and Temporal Sampling Resolutions

[50] The required sampling resolutions determine orbital coverage and along-track samplings (i.e., ''pixels''). To cover all rivers globally requires a range from about 75°N to 60°S. For a single platform with a given orbital period the repeat cycle dictates the possible temporal samplings of key hydrographs.

#### 6.3.1. Required Global Coverage

[51] Many Earth-observing satellites use a Sun-synchronous polar orbit because it provides global coverage. A dawn-dusk orbit is used to permit nonrotating solar panels, which results in a spacecraft design that does not require batteries and hence lower weight and no moving parts. One result of this orbit class is that a ~5-day repeat cycle contains 70 orbits with greater than 500-km equatorial gaps between tracks, whereas an equatorial gap spacing of less than 100 km requires ~400 revolutions or about a 30-day repeat.

[52] Spatial and temporal coverage studies were performed, as described below, using the orbits of existing satellites that operate in this Sun-synchronous mode. Pulse-limited altimeters, which are along-track profiling instruments, are contrasted with an interferometric altimeter (described in section 6.5), which provides a 120-km-wide swath of water surface heights. Comparisons are made amongst orbits of ERS-2 (35-day repeat and ~98° inclination), Terra (16-day repeat and ~98° inclination), and a generic 10-day repeat orbit (~98° inclination). This sampling study used rivers and lakes digitized in the Central Intelligence Agency World Data Bank II, an assemblage of data from the 1980s that includes river shape but not discharge (available at www.evl.uic.edu/pape/data/WDB); a University of New Hampshire time series of discharge data coregistered with the CIA database and collected from gauging stations throughout the 1970s (available at www.rivdis.sr.unh.edu); and a University of Hawaii database containing the shorelines of lakes and their areas [*Wessel and Smith*, 1996] (available at www.soest.hawaii.edu/wessel/gshhs/gshhs.html). This global compilation results in more than 6500 lakes and 3700 rivers. In the following examples it is important to note that the repeat cycle is indicative of the repeatability along a specific orbital track. For swath instruments most locations are sampled by both an ascending and a descending orbit, so the time gap between samples is closer to half of the listed repeat cycle (e.g., a 16-day repeat produces samplings every 8 days for many global areas, given an appropriately selected orbit subcycle). The same is not true of profiling instruments since ascending and descending passes only meet at crossover points, which are sparsely distributed, so that, in general, any point is only visited once during the repeat cycle. Also, the equatorial regions yield the greatest spatial and temporal gaps, compared to the poles, where orbit convergence can sometimes nearly halve the repeat observation time for swath instruments.

[53] Figures 12, 13, and 14 show the results of the coverage studies. The generic 10-day repeat orbit for a profiling altimeter results in 80% of the world's lakes remaining unsampled, whereas the swath-based altimeter yields a loss of only ~7% of the lakes. Of the ~3700 rivers, two thirds are sampled two or more times during the 10-day repeat of a swath-based altimeter, but only one third are sampled two or more times by a profiling instrument. Switching to the ERS-2 35-day repeat orbit yields complete coverage of all of the world's rivers and lakes when using a swath-based altimeter, with about 90% being sampled four or more times during the 35 days. Conversely, the profiling instrument altogether misses over half of the lakes and about 20% of the rivers. The Terra orbit falls between these two examples, with the swath instrument sampling ~90% of the world's rivers and lakes at least twice during the 16-day repeat cycle.

[54] Orbital sampling comparisons can also be made on the basis of the size of the rivers and lakes (Figures 12, 13, and 14). The generic 10-day orbit of the swath-based instrument misses only the 49th and 95th largest rivers (discharges of 3000 $m^3/s$ and 1500 $m^3/s$, respectively), whereas the profiling instrument misses 22 of the top 150 rivers (missed discharges range from 10,000 to 1000 $m^3/s$). Four lakes of the top 150 ranked by size are missed by the 10-day repeated swath instrument (largest missed lake is ~3000 $km^2$), whereas 21 lakes are missed by a profiling instrument (largest is ~8000 $km^2$). When using the ERS-2 sampling scheme, all rivers and lakes are sampled by the swath instrument, but five rivers and one lake are missed by a profiling instrument (largest missed sizes are 8000 $m^3/s$ and 300 $km^2$, respectively). The Terra orbit approach samples essentially all of the worlds rivers and lakes when using swath-based altimetry technology but, when using profiling altimeters, misses 14 and 9 of the top 150 rivers and lakes, respectively (largest missed sizes are 10,000 $m^3/s$ and 6000 $km^2$, respectively).

[55] In summary, an interferometric altimeter collecting height samples throughout a 120-km-wide swath samples all, or nearly all, of the world's rivers and lakes for any typical Sun-synchronous orbit. However, pulse-limited altimeters collecting samples only along a profile severely undersample rivers and lakes. For example, using a profiling instrument and a 16-day orbital repeat cycle, like that of Terra, misses ~30% of rivers and ~70% of lakes in the databases. Restricting the study to the largest rivers and lakes provides better coverage, but significant water bodies are still missed. Furthermore, the rivers which are covered can have only a few visits per cycle, leading to problems with slope calculations. A 120-km-swath instrument misses very few lakes or rivers: ~1% for 16-day repeat and ~7% for 10-day repeat.

#### 6.3.2. Required Local Coverage

[56] The core problem for spaceborne methods of measuring surface waters is to determine the value-added science and related costs that can be attained from various spatial (i.e., both orbital spacing and pixel size) and temporal samplings of surface water storage and movement.

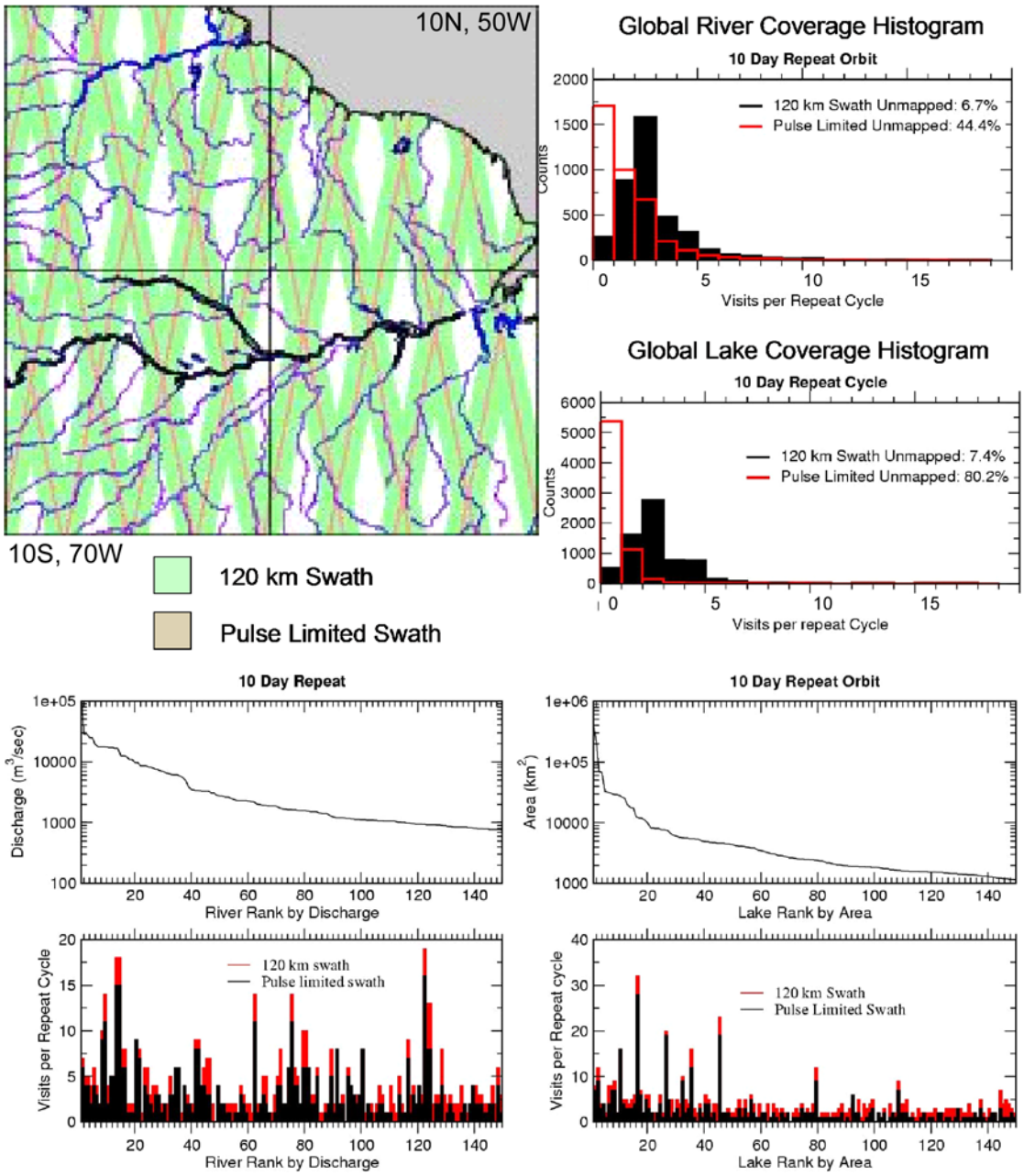


**Figure 12.** Global lake and river coverage study using a generic 10-day repeat cycle (~98° inclination and Sun-synchronous). Comparisons between profiling and imaging technologies demonstrate that 44% of the rivers and 80% of the world's lakes are missed by a profiling instrument, whereas only 7% of rivers and lakes are missed by an imager. As indicated in the bottom four plots, profiling technologies altogether miss over 20 of the world's top 150 rivers and lakes (largest missed discharge is nearly 10,000 $m^3/s$; largest missed area is ~8000 $km^2$), whereas imagers miss only two rivers and four lakes.

Specific quantitative valuations are needed to demonstrate science and cost trade-offs related to alternative spaceborne measurement approaches. This is an area of active research, but already some basic parameters are recognized. (1) To provide useful estimates of $\partial h/\partial x$, $h$ needs to be measured with an accuracy as high as several centimeters in low-gradient rivers (e.g., the Amazon River slope approaches 1.0 cm/km). Likewise, storage change estimates derived from $\partial h/\partial t$ will require centimetric $h$ accuracies (see example in section 5.2.2). (2) Spatial samplings likely will need to approach <100-m scales to measure the dynamics of flood pulses (section 5.3 and Figure 8) and the hydraulics of some river channels (e.g., the Muskingum River in Ohio drains a ~20,000 $km^2$ watershed and is less than 100 m wide [*Kiel et al.*, 2006]). (3) Temporal samplings are linked to variability in hydrographs. For example, the annual flood wave in the Amazon Basin is smooth and regular with a hydrograph that may be sampled at roughly a monthly

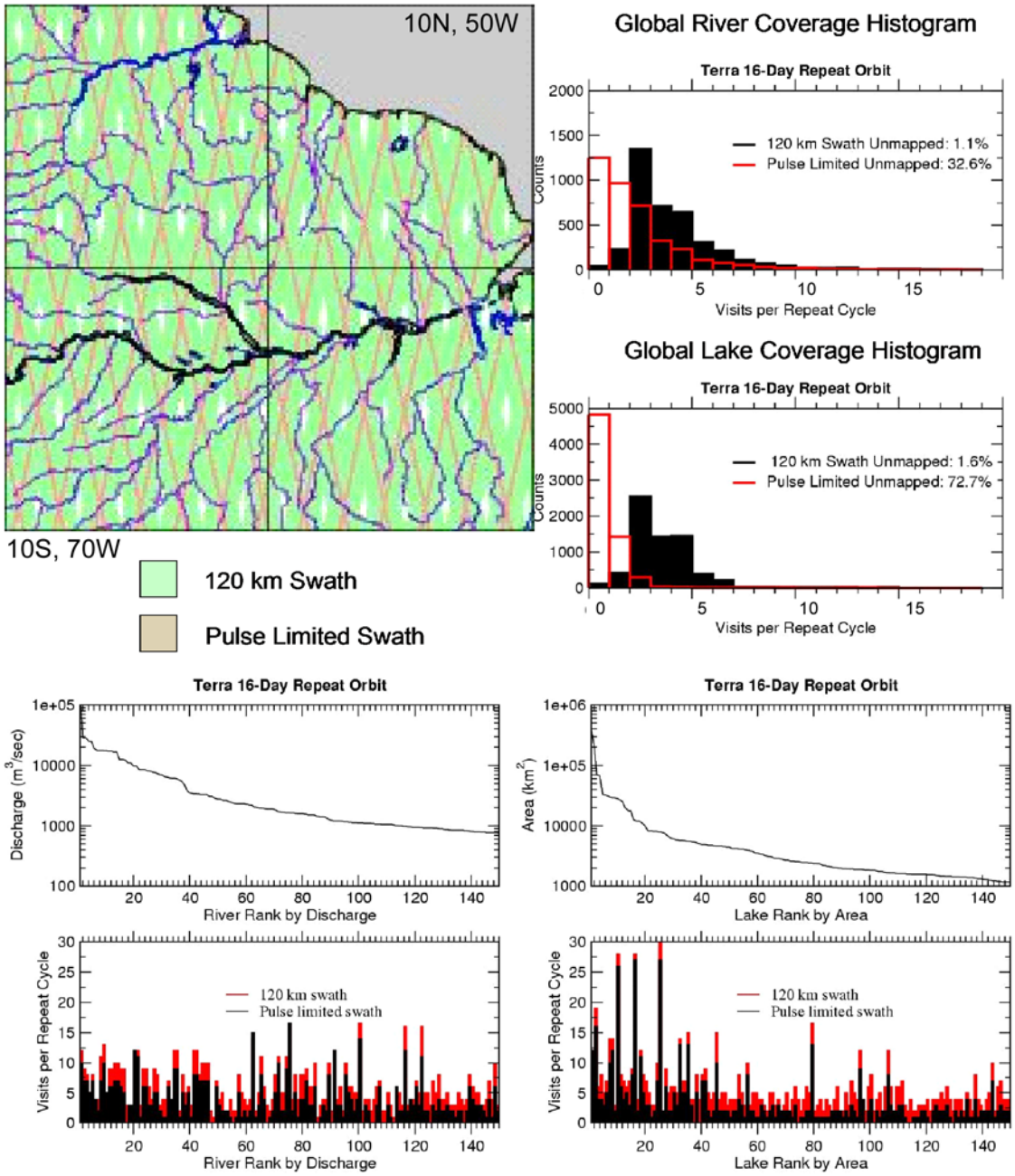


**Figure 13.** Global lake and river coverage study using Terra's 16-day repeat cycle (~98° inclination and Sun-synchronous). Comparisons between profiling and imaging technologies demonstrate that 32% of the rivers and 72% of the world's lakes are missed by a profiling instrument, whereas only 1% of rivers and lakes are missed by an imager. As indicated in the bottom four plots, profiling technologies miss altogether 14 and 9 of the world's top 150 rivers and lakes, respectively (largest missed discharge is nearly 10,000 $m^3/s$; largest missed area is ~6000 $km^2$), whereas imagers provide complete coverage.

resolution although more often is preferred. In contrast, the sudden spring melt events across the Arctic result in the bulk of the discharge occurring in a 1-month time span, or less, and hence require much more frequent (e.g., daily) sampling to capture the dynamics.

### 6.4. Future Opportunities for Estimating Discharge

[57] Data assimilation techniques have not been fully explored for surface water hydrology, especially for the estimation of model-based discharge and storage change, although early work [*Romanowicz et al.*, 2006] shows promise. Hydrodynamic flow models, such as LISFLOOD-FP [*Bates and De Roo*, 2000; *Horritt and Bates*, 2001], have already been tested against remotely sensed inundated area [e.g., *Bates et al.*, 1997]. Rather than testing the output of a flow model against a series of observations, assimilation schemes could focus on ingesting remotely sensed hydraulic data to update model predictions of discharge and storage change. This represents a fundamental contrast to the work of *Romanowicz et al.* [2006] in that satellite data

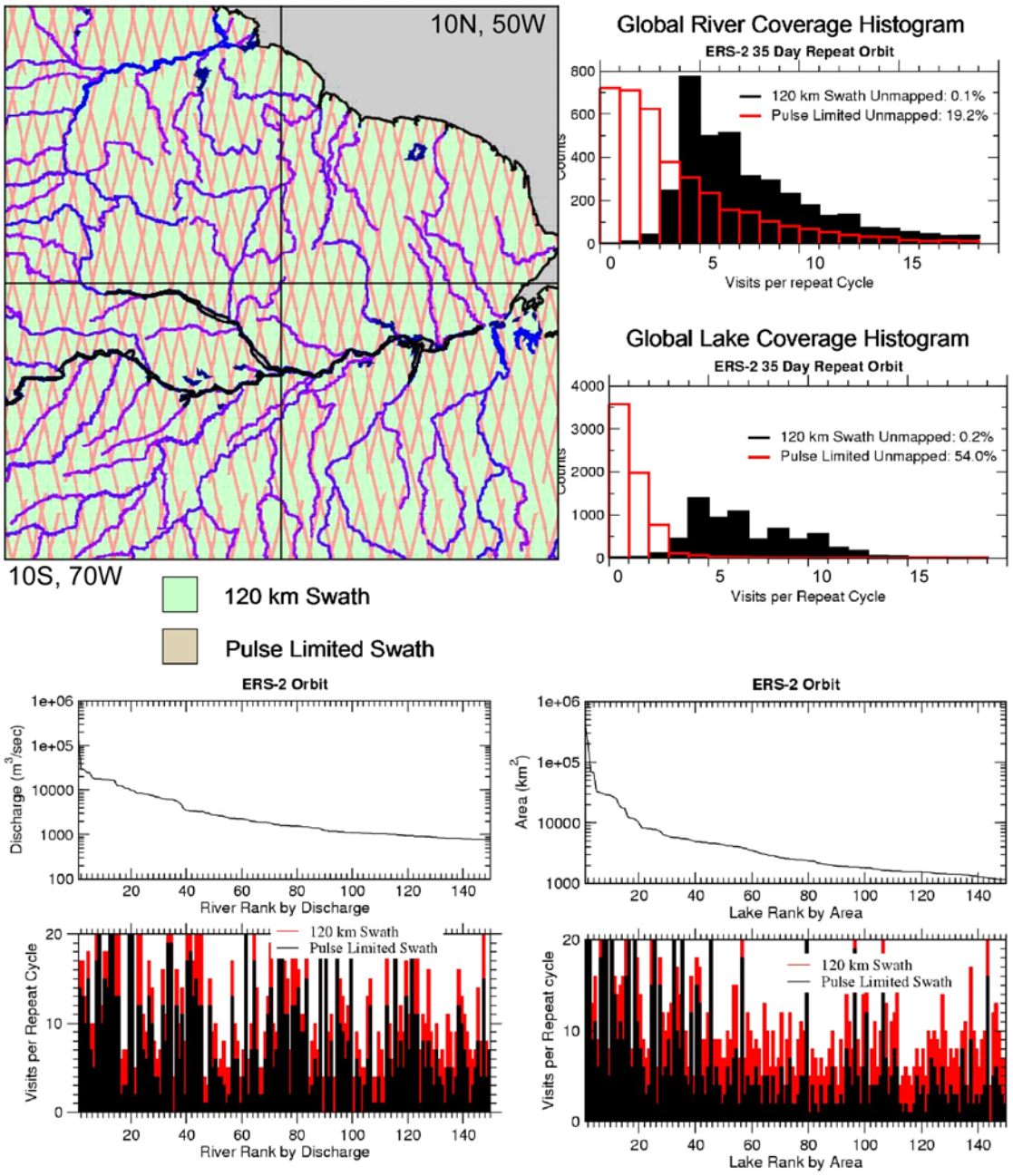


**Figure 14.** Global lake and river coverage study using the 35-day repeat cycle of ERS (~98° inclination and Sun-synchronous). Comparisons between profiling and imaging technologies demonstrate that 19% of the rivers and 54% of the world's lakes are missed by a profiling instrument, whereas far less than 1% of rivers and lakes are missed by an imager. As indicated in the bottom four plots, profiling technologies miss altogether five and one of the world's top 150 rivers and lakes, respectively (largest missed discharge is nearly 5000 $m^3/s$; largest missed area is ~300 $km^2$), whereas imagers provide complete coverage.

provide nearly spatially continuous observations at discrete times, whereas gauges provide time-continuous measurements at discrete spatial locations. A goal of the assimilation approaches required to exploit satellite altimetry data would be to determine the viability of calculating discharge by using hydraulic measurements, such as $h$, $\partial h/\partial x$, and $\partial h/\partial t$, which are proven spaceborne observations, instead of direct measurements of flow velocities and channel cross sections, which are more difficult to attain from space and unproven.

### 6.5. WATER: The Water and Terrestrial Elevation Recovery Mission Concept

[58] The Water and Terrestrial Elevation Recovery (WATER) satellite mission concept is an international effort with a large, supporting scientific community [*Mognard et al.*, 2006; *Alsdorf et al.*, 2007]. This group recognizes that the ideal instrument for measuring surface water hydraulics is a device, like that of SRTM, capable of providing image-based measurements of $h$ and its temporal ($\partial h/\partial t$) and

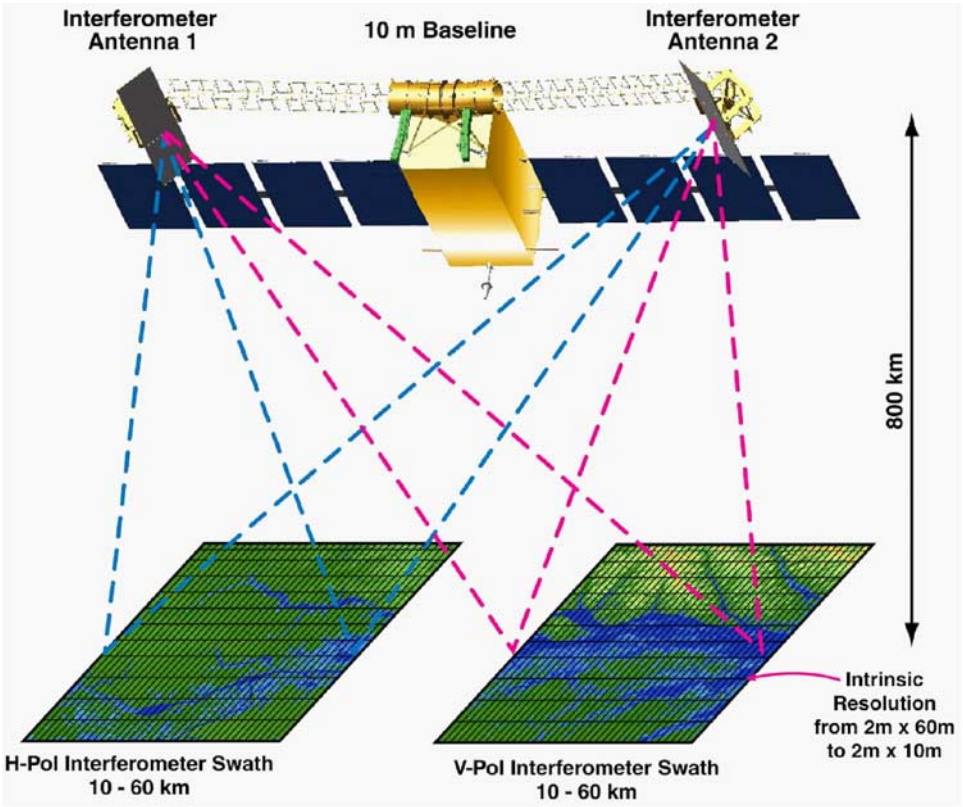


**Figure 15.** Conceptual view of KaRIN, the Ka Band Radar Interferometer, an interferometric altimeter. Maximum incidence angle is 4.3°; thus the instrument operates very near nadir where water surfaces yield strong radar returns. At Ka band the interferometer will penetrate clouds and relies on subtle canopy openings to penetrate to any underlying water surfaces (openings of only 20% are sufficient). Spatial sampling resolutions are noted in Figure 15. Height accuracies will be ±50 cm for individual "pixels"; thus centimetric accuracies are achieved through polynomial averaging methods.

spatial ($\partial h/\partial x$) derivatives. The technology for WATER is a Ka Band Radar Interferometer (KaRIN) (0.86 cm wavelength, Figure 15) (E. Rodríguez et al., Measuring freshwater levels from space using a near nadir interferometer, manuscript in preparation, 2007, hereinafter referred to as Rodríguez et al., manuscript in preparation, 2007) that has been developed from the efforts of the Wide Swath Ocean Altimeter (WSOA) [*Fu*, 2003; *Fu and Rodríguez*, 2004]. KaRIN is essentially a smaller version of SRTM with two Ka band SAR antennae at opposite ends of a 10-m boom and both antennae transmitting and receiving the emitted radar pulses along both sides of the orbital track. Look angles are limited to 4.5° providing a 120-km-wide swath. The 200-MHz bandwidth achieves cross-track ground resolutions varying from about 10 m in the far swath to about 60 m in the near swath. A resolution of about 2 m in the along-track direction is derived by means of synthetic aperture processing.

[59] The KaRIN design improves upon SRTM's meter-scale height measurements, but thermal noise limits accuracies to ~0.5 m for 10-m-sized pixels. These errors can be reduced by averaging or fitting polynomials to the $h$ values [e.g., *LeFavour and Alsdorf*, 2005]. For example, Figure 16 presents the expected height and slope performance over rivers of various widths and for a range of water surface RMS slopes (which govern water surface brightness). It was assumed for Figure 16 that at least 10 km of the river reach could be imaged and fit with a linear polynomial. It is expected that KaRIN will provide better than 5-cm accuracies for river widths of 30 m and greater. (Rodríguez et al. (manuscript in preparation, 2007) provide a description of all other error sources and strategies for their mitigation.)

[60] Many floodplain and river targets throughout the globe have inundated vegetation or vegetation along the banks that can cause either radar "layover" or signal penetration problems. Layover describes a situation when surface returns that lie at different incidence angles have the same range and therefore arrive at the same time. In this case the interferometric phase difference from the water will be contaminated by a phase noise because of the simultaneously arriving contamination from other sources. The height error due to vegetation depends on several factors: the tree height and brightness, the degree of penetration within the canopy, and the spatial density of the interferometric fringes. Fortunately, the returns from vegetation have significantly lower correlation than the returns from water because of two key factors (correlation describes the signal strength of the interferometric phase). First, vegetation

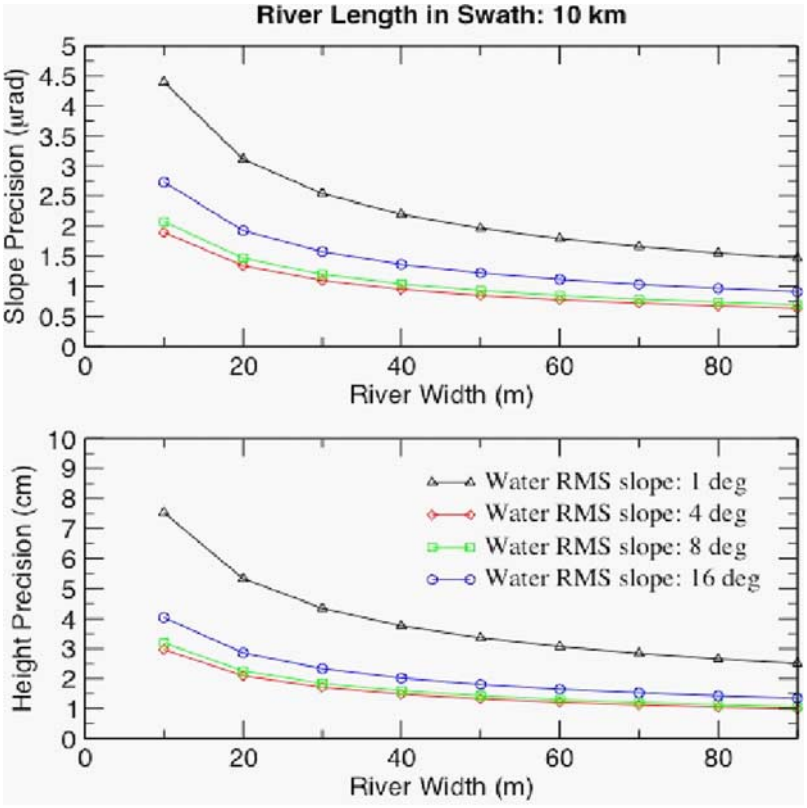


**Figure 16.** Height and slope precision of the KaRIN interferometer. Height and slope estimates are made by using the radar image to isolate water bodies and fitting a linear height change over the swath. Precision depends on water brightness and the length and width of the imaged water body.

canopies typically yield at least an order of magnitude lower backscattered radar energy than water bodies at the small look angle of KaRIN. Second, because near-nadir returns from a vegetation canopy will consist of signals arriving at the same time but from different locations in the ground (i.e., "layover") and because the near-nadir interferometric phase varies rapidly for different spatial locations [*Rodríguez and Martin*, 1992; *Rosen et al.*, 2000], the vegetation returns suffer from significant volume scattering decorrelation; that is, the vegetation returns will behave more like random noise than a correlated signal, which can bias the height estimates. To quantify this effect, we have conducted a detailed simulation of the interferometric errors for the water bodies in the Amazon Basin. The simulation is based on a mask delineating vegetation and water at a 90-m spatial resolution [*Hess et al.*, 2003], which was oversampled to a 30-m spacing. The simulation assumes that the vegetation is present everywhere with a height of 20 m and that penetration into the canopy occurs similarly to the observed penetration of other radar interferometric data, which typically report a tree height of about 60–70% of the true height [*Rosen et al.*, 2000]. This level of penetration has been observed for a large range of incidence angles from about 15° to 60°. As the incidence angle decreases, the degree of penetration increases, so that by taking the previous percentage we are examining a worst case compared to what would be observed in the near-nadir direction. We simulated three swaths of KaRIN data covering a total area of about 390,000 km$^2$. The RMS height error for the entire data set was 2.8 cm. The error was more pronounced for the smaller water bodies and for the larger incidence angles (i.e., incidence angles above 4°). Figure 17 shows the simulation extent, together with three examples of vegetation-induced errors for small water bodies of differing morphology. Although in a few extreme cases the errors can be as large as 30 cm, the performance meets the desired centimeter-scale accuracy for KaRIN. Errors can be significantly reduced by excluding the areas on the affected banks at the expense of reducing coverage.

[61] The effect of vegetation on top of water is to attenuate the signal, leading to a noisier return. The amount of penetration into vegetation canopies in the near nadir direction will be no worse than that of optical instruments, such as the ICESat altimeter, which have demonstrated penetration even for tropical canopies [e.g., *Schutz et al.*, 2005]. The main impact of vegetation over water will be to decrease the ability to distinguish between the two when looking at the radar brightness. Since water is much brighter than vegetation at small look angles, the requirement that inundation extent be detectable will be possible as long as the fraction of canopy gaps times the ratio of water to land brightness is greater than about 2. This leads to a requirement that the canopy have a fraction of gaps greater than about 20%, which is true for all but the heaviest canopies.

[62] The technological heritage of KaRIN comes from the oceanographic (WSOA) and terrestrial (SRTM) mapping communities. Community building is essential for today's

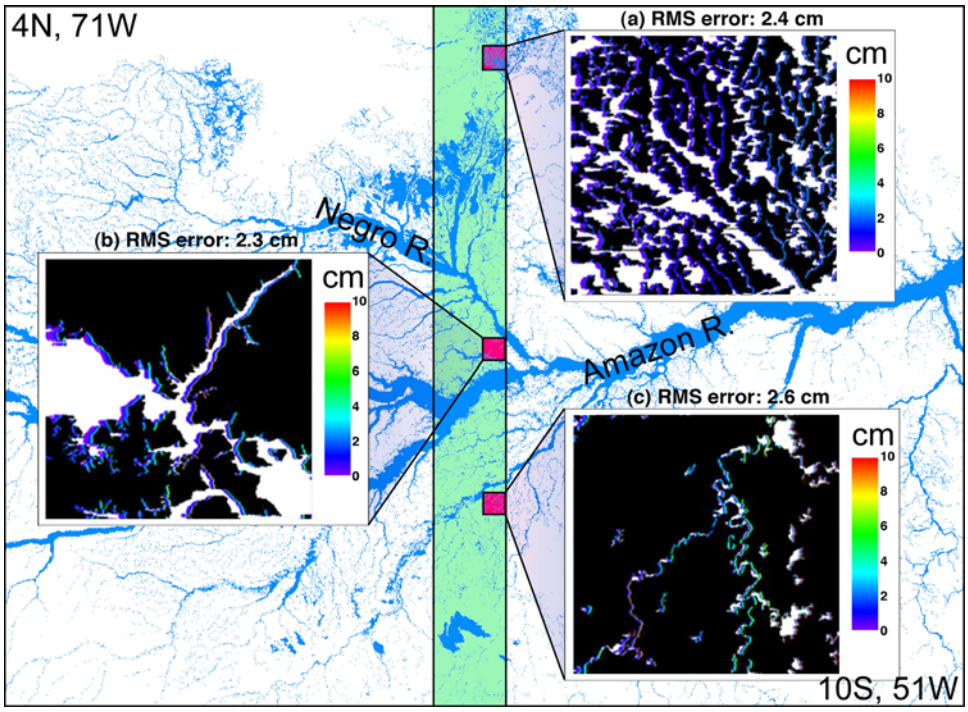


**Figure 17.** Vegetation layover effects simulated in a KaRIN swath (green vertical rectangle). The area in green shows the region used to simulate the effect of vegetation on KaRIN's interferometric heights for a region in the Amazon Basin. The water mask is the background, with blue indicative of water and white marking land. Three 15-km$^2$ areas are magnified, each containing small rivers and wetlands of differing morphology. When the instrument looks from the left (west), the effects of layover errors are located on the right (east) banks of the water bodies. In the far range (east side of the swath) the errors can be larger than in the near (west) side because of higher volumetric correlation of the vegetation returns. The root mean square error for the entire simulation is 2.8 cm, assuming that the water was 10 times brighter than the vegetation.

satellite missions, suggesting the following potential collaborative science opportunities with WATER. (1) Many floodplains experience dry conditions when their topography is exposed. The interferometric altimeter could repeatedly sample these locations with decimeter-scale-sized pixels, which when temporally averaged over the lifespan of a mission, will provide centimeter-scale height accuracies. Given that a mission would extend to 75°N (minimally), it will also help supplement the SRTM database, which extends to 60°N. (2) Nearshore ocean surface elevations are poorly known because existing oceanic altimeters lack the required between-track spacing. KaRIN's swath would blanket coastal zones with $h$ measurements. (3) Mesoscale ocean circulation patterns are poorly known, but the swath mode of the interferometric altimeter permits a dense sampling that can be used to infer these patterns. Similarly, ocean bathymetry could be estimated from dense samplings of water surface topography. (4) Sea ice freeboard could also be mapped by comparing the elevations across the top of floating ice to the surrounding ocean elevations.

## 7. CONCLUSIONS

[63] Remotely measuring surface water hydraulics from space has greatly improved over the past decade. For example, radar altimetry has been demonstrated to be a viable method for collecting water surface elevation measurements along orbital profiles, whereas interferometric processing of SAR data has recently been used to map temporal changes in water levels at a high spatial resolution. SRTM provided the first ever two-dimensional spaceborne measurements of water surfaces, i.e., images of $h$. These advances point to future opportunities and key challenges. (1) Because discharge estimation relies, in part, on knowledge of cross-sectional channel geometry yet bathymetry remains unlikely to be measured from space, what are the discharge error limits when using spaceborne measurements of $h$, $\partial h/\partial t$, and $\partial h/\partial x$ that can be remotely measured (section 6.4)? (2) The spacings of conventional altimetry orbital tracks miss too many of the world's freshwater bodies (section 6.3.1), suggesting instead that swath-based mapping of water surface elevations is required to address key hydrologic questions (section 3). However, what are the required spatial and temporal resolutions? Are weekly, ~100-m samplings sufficient, inadequate, or excessive? (3) Current technology allows a satellite mission to map the elevations of surface waters across the globe and to derive storage changes in lakes, reservoirs, and wetlands and the discharge of major rivers (section 6.5). The heritage of a suggested technology, KaRIN, is from communities concerned with ocean water surfaces and terrestrial elevations.

Ideally, these groups will combine with hydrologists to pool strengths and work toward a mutually beneficial satellite mission.

[64] **ACKNOWLEDGMENTS.** We thank the participants in the proposed WATER mission and the members of the NASA SWWG for their interactions and sharing of ideas. Their collegiality is a cornerstone of these successful groups. D. Alsdorf and D. Lettenmaier are funded by NASA's Terrestrial Hydrology Program; E. Rodríguez is supported by the Jet Propulsion Laboratory, California Institute of Technology, Pasadena, California, under a contract with NASA. We sincerely thank D. Moller, JPL, for many technical discussions related to the KaRIN instrument and especially N. Mognard of CNES for her leadership of WATER in Europe.

[65] The Editor responsible for this paper was Daniel Tartakovsky. He thanks technical reviewers Anny Cazenave and Tom Farr and an anonymous reviewer.

## REFERENCES

Albertson, M. L., and D. B. Simons (1964), Fluid mechanics, in *Handbook of Applied Hydrology: A Compendium of Water-Resources Technology*, edited by V. T. Chow, McGraw-Hill, New York.

Alpers, W. (1985), Theory of radar imaging of internal waves, *Nature*, *314*, 245–247.

Alsdorf, D. E. (2003), Water storage of the central Amazon floodplain measured with GIS and remote sensing imagery, *Ann. Assoc. Am. Geogr.*, *93*, 55–66.

Alsdorf, D. E. (2004), A new view of Amazon floodplain hydraulics, *Eos Trans. AGU*, *85*(47), Fall Meet. Suppl., Abstract H23E-1179.

Alsdorf, D. E., and D. P. Lettenmaier (2003), Tracking fresh water from space, *Science*, *301*, 1485–1488.

Alsdorf, D. E., J. M. Melack, T. Dunne, L. A. K. Mertes, L. L. Hess, and L. C. Smith (2000), Interferometric radar measurements of water level changes on the Amazon floodplain, *Nature*, *404*, 174–177.

Alsdorf, D. E., L. C. Smith, and J. M. Melack (2001a), Amazon floodplain water level changes measured with interferometric SIR-C radar, *IEEE Trans. Geosci. Remote Sens.*, *39*, 423–431.

Alsdorf, D., C. Birkett, T. Dunne, J. Melack, and L. Hess (2001b), Water level changes in a large Amazon lake measured with spaceborne radar interferometry and altimetry, *Geophys. Res. Lett.*, *28*, 2671–2674.

Alsdorf, D., D. Lettenmaier, C. Vörösmarty, and the NASA Surface Water Working Group (2003), The need for global, satellite-based observations of terrestrial surface waters, *Eos Trans. AGU*, *84*(29), 275–276.

Alsdorf, D., E. Rodríguez, D. Lettenmaier, and J. Famiglietti (2007), WatER: The Water Elevation Recovery satellite mission, a response to the National Research Council Decadal Survey Request for Information, in *Earth Science and Applications From Space: National Imperatives for the Next Decade and Beyond*, Nat. Res. Counc., Washington, D. C., in press.

Banic, J. R., and A. G. Cunningham (1998), Airborne laser bathymetry: A tool for the next millennium, *EEZ Technol.*, *3*, 75–80.

Bates, P. D., and A. P. J. De Roo (2000), A simple raster-based model for floodplain inundation, *J. Hydrol.*, *236*, 54–77.

Bates, P. D., M. S. Horritt, C. N. Smith, and D. Mason (1997), Integrating remote sensing observations of flood hydrology and hydraulic modelling, *Hydrol. Processes*, *11*, 1777–1795.

Birkett, C. M. (1995), The contribution of TOPEX/Poseidon to the global monitoring of climatically sensitive lakes, *J. Geophys. Res.*, *100*, 25,179–25,204.

Birkett, C. M. (1998), Contribution of the TOPEX NASA radar altimeter to the global monitoring of large rivers and wetlands, *Water Resour. Res.*, *34*, 1223–1239.

Birkett, C., and B. Doorn (2004), A new remote-sensing tool for water resources management, *Earth Obs. Mag.*, *13*, 20–21.

Birkett, C. M., L. A. K. Mertes, T. Dunne, M. H. Costa, and M. J. Jasinski (2002), Surface water dynamics in the Amazon Basin: Application of satellite radar altimetry, *J. Geophys. Res.*, *107*(D20), 8059, doi:10.1029/2001JD000609.

Bjerklie, D. M., S. L. Dingman, C. J. Vörösmarty, C. H. Bolster, and R. G. Congalton (2005a), Evaluating the potential for measuring river discharge from space, *J. Hydrol.*, *278*, 17–38.

Bjerklie, D. M., D. Moller, L. Smith, and L. Dingman (2005b), Estimating discharge in rivers using remotely sensed hydraulic information, *J. Hydrol.*, *309*, 191–209.

Brakenridge, G. R., S. V. Nghiem, E. Anderson, and S. Chien (2005), Space-based measurement of river runoff, *Eos Trans. AGU*, *86*(19), 185–188.

Cazenave, A., P. C. D. Milly, H. Douville, J. Benveniste, P. Kosuth, and D. Lettenmaier (2004), Space techniques used to measure change in terrestrial waters, *Eos Trans. AGU*, *85*(6), 59.

Coe, M. T. (2000), Modeling terrestrial hydrological systems at the continental scale: Testing the accuracy of an atmospheric GCM, *J. Clim.*, *13*, 686–704.

Costa, J. E., K. R. Spicer, R. T. Cheng, F. P. Haeni, N. B. Melcher, E. M. Thurman, W. J. Plant, and W. C. Keller (2000), Measuring stream discharge by non-contact methods: A proof-of-concept experiment, *Geophys. Res. Lett.*, *27*, 553–556.

Costa, J. E., R. T. Cheng, F. P. Haeni, N. Melcher, K. R. Spicer, E. Hayes, W. Plant, K. Hayes, C. Teague, and D. Barrick (2006), Use of radars to monitor stream discharge by noncontact methods, *Water Resour. Res.*, *42*, W07422, doi:10.1029/2005WR004430.

Cretaux, J.-F., A. V. Kouraev, F. Papal, M. Bergé-Nguyen, A. Cazenave, N. Aladin, and I. S. Plotnikov (2005), Evolution of sea level of the Big Aral Sea from satellite altimetry and its implications for water balance, *J. Great Lakes Res.*, *31*, 520–534.

Davis, P. A. (2004), Review of results and recommendations from the GCMRC 2000–2003 remote-sensing initiative for monitoring environmental resources within the Colorado River ecosystem, *U. S. Geol. Surv. Open File Rep., 2004-1206.* (Available at http://pubs.usgs.gov/of/2004/1206/)

Emmitt, G. D., and M. Kavaya (2001), Ocean and river current observations using CDWL, paper presented at 11th Coherent Laser Radar Conference, Amey Imager, Malvern, U. K.

Farr, T., et al. (2007), The Shuttle Radar Topography Mission, *Rev. Geophys.*, doi:10.1029/2005RG000183, in press.

Frappart, F., S. Calmant, M. Cauhope, F. Seyler, and A. Cazenave (2006), Preliminary results of ENVISAT RA-2–derived water levels validation over the Amazon Basin, *Remote Sens. Environ.*, *100*, 252–264.

Frey, K. E., and L. C. Smith (2005), Amplified carbon release from vast west Siberian peatlands by 2100, *Geophys. Res. Lett.*, *32*, L09401, doi:10.1029/2004GL022025.

Frey, K. E., and L. C. Smith (2007), How well do we know northern land cover? Comparison of four global vegetation and wetland products with a new ground-truth database for west Siberia, *Global Biogeochem. Cycles*, *21*, GB1016, doi:10.1029/2006GB002706.

Fu, L.-L. (Ed.) (2003), Wide-swath altimetric measurement of ocean surface topography, *JPL Publ., 03-002,* 67 pp. (Available at ftp://oceans.jpl.nasa.gov/pub/llf/WSOAreportFinal2.pdf)

Fu, L.-L., and E. Rodriguez (2004), High-resolution measurement of ocean surface topography by radar interferometry for oceanographic and geophysical applications, in *The State of the Planet: Frontiers and Challenges in Geophysics*, *Geophys. Monogr. Ser.*, vol. 150, edited by R. S. J. Sparks and C. J. Hawkesworth, pp. 209–224, AGU, Washington, D. C.

Gleick, P. H. (2003), Global freshwater resources: Soft-path solutions for the 21st century, *Science*, *302*, 1524–1528.

Goldstein, R. M., and H. A. Zebker (1987), Interferometric radar measurement of ocean surface currents, *Nature*, *328*, 707–709.

Goldstein, R. M., T. P. Barnett, and H. A. Zebker (1989), Remote sensing of ocean currents, *Science*, *246*, 1282–1285.

Han, S. C., C. K. Shum, C. Jekeli, and D. Alsdorf (2005), Improved estimation of terrestrial water storage changes from GRACE, *Geophys. Res. Lett.*, *32*, L07302, doi:10.1029/2005GL022382.

Harding, D., and M. Jasinski (2004), ICESat observations of inland surface water stage, slope, and extent: A new method for hydrologic monitoring, *Eos Trans. AGU*, *85*(47), Fall Meet. Suppl., Abstract C21B-05.

Hess, L. L., J. M. Melack, S. Filoso, and Y. Wang (1995), Delineation of inundated area and vegetation along the Amazon floodplain with SIR-C synthetic aperture radar, *IEEE Trans. Geosci. Remote Sens.*, *33*, 896–904.

Hess, L. L., J. M. Melack, E. M. L. M. Novo, C. C. F. Barbosa, and M. Gastil (2003), Dual-season mapping of wetland inundation and vegetation for the central Amazon Basin, *Remote Sens. Environ.*, *87*, 404–428.

Horritt, M. S. (2000), Calibration of a two-dimensional finite element flood flow model using satellite radar imagery, *Water Resour. Res.*, *36*, 3279–3291.

Horritt, M. S., and P. D. Bates (2001), Effects of spatial resolution on a raster based model of flood flow, *J. Hydrol.*, *253*, 239–249.

Hwang, C., M.-F. Peng, J. Ning, J. Luo, and C.-H. Sui (2005), Lake level variations in China from TOPEX/Poseidon altimetry: Data quality assessment and links to precipitation and ENSO, *Geophys. J. Int.*, *161*, 1–11.

International Working Group on Earth Observations (2005), Strategic plan for the U.S. integrated earth observation system, report, 166 pp., Natl. Sci. and Technol. Counc., Washington, D. C. (Available at www.ostp.gov/html/EOCStrategic_Plan.pdf)

Jacobson, R. B., and K. A. Oberg (1997), Geomorphic changes of the Mississippi River floodplain at Miller City, Illinois, as a result of the flood of 1993, *U.S. Geol. Surv. Circ.*, *1120-J*.

Kiel, B., D. Alsdorf, and G. LeFavour (2006), Capability of SRTM C and X band DEM data to measure water elevations in Ohio and the Amazon, *Photogramm. Eng. Remote Sens.*, *72*, 313–320.

Kim, S. W., S. H. Hong, and J. S. Won (2005), An application of L-band synthetic aperture radar to tide height measurement, *IEEE Trans. Geosci. Remote Sens.*, *43*, 1472–1478.

Kouraev, A. V., E. A. Zakharovab, O. Samainc, N. M. Mognard, and A. Cazenave (2004), Ob' River discharge from TOPEX/Poseidon satellite altimetry (1992–2002), *Remote Sens. Environ.*, *93*, 238–245.

LeFavour, G., and D. Alsdorf (2005), Water slope and discharge in the Amazon River estimated using the shuttle radar topography mission digital elevation model, *Geophys. Res. Lett.*, *32*, L17404, doi:10.1029/2005GL023836.

Leon, J. G., S. Calmant, F. Seyler, M.-P. Bonnet, M. Cauhopé, F. Frappart, N. Filizola, and P. Fraizy (2007), Rating curves and estimation of average water depth at the upper Negro River based on satellite altimeter data and modeled discharges, *J. Hydrol.*, *328*, 481–496.

Leopold, L. B., and T. Maddock (1953), The hydraulic geometry of stream channels and some physiographic implications, *U.S. Geol. Surv. Prof.*, (252).

Leopold, L. B., M. G. Wolman, and J. P. Miller (1964), *Fluvial Processes in Geomorphology*, Dover, Mineola, N. Y.

Lettenmaier, D. P. (2005), Observations of the global water cycle—Global monitoring networks, in *Encyclopedia of Hydrologic Sciences*, vol. 5, edited by M. G. Anderson and J. J. McDonnell, pp. 2719–2732, John Wiley, Hoboken, N. J.

Lu, Z., M. Crane, O. Kwoun, C. Wells, C. Swarzenski, and R. Rykhus (2005), C-band radar observes water level change in swamp forests, *Eos Trans. AGU*, *86*(14), 141–144.

Maheu, C., A. Cazenave, and C. R. Mechoso (2003), Water level fluctuations in the Plata Basin (South America) from TOPEX/Poseidon satellite altimetry, *Geophys. Res. Lett.*, *30*(3), 1143, doi:10.1029/2002GL016033.

Marburger, J. H., and J. B. Bolten (2004), Administration research and development budget priorities, *Memo. M-04-23,* Executive Off. of U.S. Pres., Washington, D. C. (Available at http://www.whitehouse.gov/omb/memoranda/fy04/m04-23.pdf.)

Marburger, J. H., and J. B. Bolten (2005), FY 2007 administration research and development budget priorities, *Memo. M-05-18*, Executive Off. of U.S. Pres., Washington, D. C. (Available at http://www.ostp.gov/html/budget/2007/ostp_omb_guidancememo_FY07.pdf.)

Matthews, E., and I. Fung (1987), Methane emission from natural wetlands: Global distribution, area, and environmental characteristics of sources, *Global Biogeochem. Cycles*, *1*, 61–86.

Mayaux, P., G. F. De Grandi, Y. Rauste, M. Simard, and S. Saatchi (2002), Large-scale vegetation maps derived from the combined L-band GRFM and C-band CAMP wide area radar mosaics of central Africa, *Int. J. Remote Sens.*, *23*, 1261–1282.

Melack, J. M., and B. R. Forsberg (2001), Biogeochemistry of Amazon floodplain lakes and associated wetlands, in *The Biogeochemistry of the Amazon Basin*, edited by M. E. McClain, R. L. Victoria, and J. E. Richey, pp. 235–274, Oxford Univ. Press, New York.

Mercier, F., A. Cazenave, and C. Maheu (2002), Interannual lake level fluctuations (1993–1999) in Africa from TOPEX/Poseidon: Connections with ocean-atmosphere interactions over the Indian Ocean, *Global Planet. Change*, *32*, 141–163.

Mertes, L. A. K. (1997), Documentation and significance of the perirheic zone on inundated floodplains, *Water Resour. Res.*, *33*, 1749–1762.

Mertes, L. A. K. (2002), Remote sensing of riverine landscapes, *Freshwater Biol.*, *47*, 799–816.

Mertes, L. A. K., D. L. Daniel, J. M. Melack, B. Nelson, L. A. Martinellie, and B. R. Forsberg (1995), Spatial patterns of hydrology, geomorphology, and vegetation on the floodplain of the Amazon River in Brazil from a remote sensing perspective, *Geomorphology*, *13*, 215–232.

Mognard, N. M., et al. (2006), WatER: The Water Elevation Recovery satellite mission, paper presented at 15 Years of Progress in Radar Altimetry Symposium, Eur. Space Agency, 13–18 March.

Moussa, R., and C. Bocquillon (1996), Criteria for the choice of flood-routing methods in natural channels, *J. Hydrol.*, *186*, 1–30.

National Science and Technology Council (2004), Science and technology to support fresh water availability in the United States, report, Washington, D. C. (Available at www.ostp.gov/NSTC/html/swaqreport_2-1-05.pdf)

Ngo-Duc, T., K. Laval, G. Ramillien, J. Polcher, and A. Cazenave (2007), Validation of the land water storage simulated by Organising Carbon and Hydrology in Dynamic Ecosystems (ORCHIDEE) with Gravity Recovery and Climate Experiment (GRACE) data, *Water Resour. Res.*, *43*, W04427, doi:10.1029/2006WR004941.

Papa, F., C. Prigent, F. Durand, and W. B. Rossow (2006), Wetland dynamics using a suite of satellite observations: A case study of application and evaluation for the Indian subcontinent, *Geophys. Res. Lett.*, *33*, L08401, doi:10.1029/2006GL025767.

Peterson, B. J., R. M. Holmes, J. W. McClelland, C. J. Vörösmarty, R. B. Lammers, A. I. Shiklomanov, I. A. Shiklomanov, and S. Rahmstorf (2002), Increasing river discharge to the Arctic Ocean, *Science*, *298*, 2171–2173.

Plant, W., W. Keller, and K. Hayes (2005), Measurement of river surface currents with coherent microwave systems, *IEEE Trans. Geosci. Remote Sens.*, *43*, 1242–1257.

Prigent, C., E. Matthews, F. Aires, and W. Rossow (2001), Remote sensing of global wetland dynamics with multiple satellite data sets, *Geophys. Res. Lett.*, *28*, 4631–4634.

Ramillien, G., F. Frappart, A. Cazenave, and A. Guntner (2005), Time variations of land water storage from an inversion of 2 years of GRACE geoids, *Earth Planet. Sci. Lett.*, *235*, 283–301.

Richey, J. E., L. A. K. Mertes, T. Dunne, R. L. Victoria, B. R. Forsberg, A. C. N. S. Tancredi, and E. Oliveira (1989), Sources and routing of the Amazon River flood wave, *Global Biogeochem. Cycles*, *3*, 191–204.

Richey, J. E., J. M. Melack, A. K. Aufdenkampe, V. M. Ballester, and L. L. Hess (2002), Outgassing from Amazonian rivers and wetlands as a large tropical source of atmospheric $CO_2$, *Nature*, *416*, 617–620.

Roads, J., et al. (2003), GCIP Water and Energy Budget Synthesis (WEBS), *J. Geophys. Res.*, *108*(D16), 8609, doi:10.1029/2002JD002583.

Robinson, J. S., and M. Sivapalan (1997), An investigation into the physical causing of scaling and heterogeneity of regional flood frequency, *Water Resour. Res.*, *33*, 1045–1059.

Rodell, M., and J. S. Famiglietti (1999), Detectability of variations in continental water storage from satellite observations of the time dependent gravity field, *Water Resour. Res.*, *35*, 2705–2723.

Rodell, M., and J. S. Famiglietti (2001), An analysis of terrestrial water storage variations in Illinois with implications for the Gravity Recovery and Climate Experiment (GRACE), *Water Resour. Res.*, *37*, 1327–1339.

Rodríguez, E., and J. M. Martin (1992), Theory and design of interferometric SARs, *Proc. IEEE*, *139*, 147–159.

Rodríguez, E., C. S. Morris, and J. E. Belz (2006), A global assessment of the SRTM performance, *Photogramm. Eng. Remote Sens.*, *72*, 249–260.

Romanowicz, R. J., P. C. Young, and K. J. Beven (2006), Data assimilation and adaptive forecasting of water levels in the river Severn catchment, United Kingdom, *Water Resour. Res.*, *42*, W06407, doi:10.1029/2005WR004373.

Romeiser, R., J. Sprenger, D. Stammer, H. Runge, and S. Suchandt (2005), Global current measurements in rivers by spaceborne along-track InSAR, paper presented at IGARSS—2005 International Geosciences and Remote Sensing Symposium, Inst. of Electr. and Electron. Eng., Seoul, South Korea.

Rosen, P. A., S. Hensley, I. R. Joughin, F. K. Li, S. N. Madsen, E. Rodríguez, and R. M. Goldstein (2000), Synthetic aperture radar interferometry: Invited paper, *Proc. IEEE*, *88*, 333–382.

Rosenqvist, A., M. Shimada, B. Chapman, L. Dutra, S. Saatchi, and O. Tanaka (2002), The Global Rain Forest Mapping project: Introduction from guest editors, *Int. J. Remote Sens.*, *23*, 1215.

Sanders, R. E. (1992), Day versus night electrofishing catches from near-shore waters of the Ohio and Muskingum rivers, *Ohio J. Sci.*, *92*, 51–59.

Schmidt, M., S.-C. Han, J. Kusche, I. Sanchez, and C. K. Shum (2006), Regional high-resolution spatiotemporal gravity modeling from GRACE data using spherical wavelets, *Geophys. Res. Lett.*, *33*, L08403, doi:10.1029/2005GL025509.

Schutz, B. E., H. J. Zwally, C. A. Shuman, D. Hancock, and J. P. DiMarzio (2005), Overview of the ICESat mission, *Geophys. Res. Lett.*, *32*, L21S01, doi:10.1029/2005GL024009.

Shiklomanov, A. I., R. B. Lammers, and C. J. Vörösmarty (2002), Widespread decline in hydrological monitoring threatens Pan-Arctic research, *Eos Trans. AGU*, *83*(2), 13–16.

Sippel, S. J., S. K. Hamilton, J. M. Melack, and E. M. M. Novo (1998), Passive microwave observations of inundation area and the area/stage relation in the Amazon River floodplain, *Int. J. Remote Sens.*, *19*, 3055–3074.

Smith, L. C. (1997), Satellite remote sensing of river inundation area, stage, and discharge: A review, *Hydrol. Processes*, *11*, 1427–1439.

Smith, L. C., and D. E. Alsdorf (1998), Control on sediment and organic carbon delivery to the Arctic Ocean revealed with spaceborne synthetic aperture radar: Ob' River, Siberia, *Geology*, *26*, 395–398.

Smith, L. C., B. L. Isacks, R. R. Forster, A. L. Bloom, and I. Preuss (1995), Estimation of discharge from braided glacial rivers using ERS-1 SAR: First results, *Water Resour. Res.*, *31*, 1325–1329.

Smith, L. C., B. L. Isacks, A. L. Bloom, and A. B. Murray (1996), Estimation of discharge from three braided rivers using synthetic aperture radar (SAR) satellite imagery: Potential application to ungaged basins, *Water Resour. Res.*, *32*, 2021–2034.

Smith, L. C., Y. Sheng, G. M. MacDonald, and L. D. Hinzman (2005), Disappearing Arctic lakes, *Science*, *308*, 1429, doi:10.1126/science.1108142.

Sridhar, V., G. Goteti, J. Sheffield, E. F. Wood, D. P. Lettenmaier, and C. M. Birkett (2003), Evaluating the variability and budgets of global water cycle components, paper presented at 14th Symposium on Global Change and Climate Variations, Am. Meteorol. Soc., Long Beach, Calif., 9–13 Feb.

Stedinger, J. R., R. M. Vogel, and E. Foufoula-Georgiou (1993), Frequency analysis of extreme events, in *Handbook of Hydrology*, edited by D. R. Maidment, pp. 18.1–18.66, McGraw-Hill, New York.

Stokstad, E. (1999), Scarcity of rain, stream gages threatens forecasts, *Science*, *285*, 1199, doi:10.1126/science.285.5431.1199.

Swenson, S., and P. C. D. Milly (2006), Climate model biases in seasonality of continental water storage revealed by satellite gravimetry, *Water Resour. Res.*, *42*, W03201, doi:10.1029/2005WR004628.

Tapley, B. D., S. Bettadpur, J. C. Ries, P. F. Thompson, and M. M. Watkins (2004), GRACE measurements of mass variability in the Earth system, *Science*, *305*, 503–505.

Thompson, L. G., T. Yao, E. Mosley-Thompson, M. E. Davis, K. A. Henderson, and P.-N. Lin (2000), A high-resolution millennial record of the south Asian monsoon from Himalayan ice cores, *Science*, *289*, 1916–1919.

United Nations (2004), International Decade for Action, "Water for Life," 2005–2015, *Gen. Assem. Resolut. A/RES/58/217*, New York. (Available at www.un.org/Depts/dhl/resguide/r58.htm.)

Vance, J. M. (1994), Plugging up the drain, *Mo. Conserv.*, *55*, 22–27.

Vörösmarty, C. J., C. J. Willmott, B. J. Choudhury, A. L. Schloss, T. K. Stearns, S. M. Robeson, and T. J. Dorman (1996), Analyzing the discharge regime of a large tropical river through remote sensing, ground-based climatic data, and modeling, *Water Resour. Res.*, *32*, 3137–3150.

Vörösmarty, C. J., P. Green, J. Salisbury, and R. B. Lammers (2000), Global water resources: Vulnerability from climate changes and population growth, *Science*, *289*, 284–288.

Vörösmarty, C., et al. (2001), Global water data: A newly endangered species, *Eos Trans. AGU*, *82*(5), 56–58.

Wahr, J., M. Molenaar, and F. Bryan (1998), Time-variability of the Earth's gravity field: Hydrological and oceanic effects and their possible detection using GRACE, *J. Geophys. Res.*, *103*, 30,205–30,230.

Wahr, J., S. Swenson, V. Zlotnicki, and I. Velicogna (2004), Time-variable gravity from GRACE: First results, *Geophys. Res. Lett.*, *31*, L11501, doi:10.1029/2004GL019779.

Wessel, P., and W. H. F. Smith (1996), A global self-consistent, hierarchical, high-resolution shoreline database, *J. Geophys. Res.*, *101*, 8741–8743.

Wozencraft, J. M., and W. J. Lillycrop (2002), Total shallow-water survey through airborne hydrography, paper presented at Oceanology International 2002, Southampton Oceanogr. Cent., London, U. K.

Zakharova, E. A., A. V. Kouraev, A. Cazenave, and F. Seyler (2006), Amazon River discharge estimated from the TOPEX/Poseidon altimetry, *C. R. Geosci.*, *338*, 188–196.

D. E. Alsdorf, School of Earth Sciences, Ohio State University, 383 Mendenhall Laboratory, 125 South Oval Mall, Columbus, OH 43210-1808 USA. (alsdorf1@osu.edu)

D. P. Lettenmaier, Department of Civil and Environmental Engineering, University of Washington, Seattle, Box 352700, WA 98195-2700, USA.

E. Rodríguez, Jet Propulsion Laboratory, California Institute of Technology, Pasadena, CA 91109, USA.